

1 **Responses to the Comments of Referee #1**

2
3 **(1)** Organic aerosol (OA) is an important aerosol component in the atmosphere. One key
4 to fully understanding OA is to constrain the volatility and hygroscopicity of OA. This
5 manuscript used the measurements by a thermodenuder coupled with a HR-AMS to
6 analyze OA source, volatility distribution, oxidation state and hygroscopicity. This study
7 gives the OA community some insights on OA volatility and hygroscopicity, and pointed
8 out the caveat of deriving the volatility of OA only from its mass fraction remaining
9 (MFR). These findings are worth publishing for sure.

10 We do appreciate the positive assessment of our work. The responses to each comment of
11 the reviewer and the corresponding changes in the manuscript can be found below.

12
13 **(2)** I don't have many comments but hope the authors can explain why they only used 3-
14 bin C* distribution (rather than 5 bins, 10 bins, for example) to fit the measured
15 thermograms. 3 bins cannot cover the whole range of real OA volatilities. Also, can the
16 authors describe more on the approach of Karnezi et al. (2014) that was used to calculate
17 the best fit of MFR and the uncertainties of OA volatility distributions? I find it hard to
18 understand this method based on the current form.

19 The number of bins that can be used in the analysis of thermodenuder data is in general
20 determined by the ambient OA concentration (the bin range can extend up to an order of
21 magnitude higher than the measured values), the number of temperature steps used in the
22 analysis (the number of bins cannot be much higher than the number of data points
23 available for fitting), and the maximum fraction of the OA evaporated during the analysis.
24 Our selection of only 3 bins was determined by the availability of measurements at 25, 60,
25 80 and 100 C. The concentration of the OA was of the order of $5 \mu\text{g m}^{-3}$, so there is a
26 little information about compounds with saturation concentration of $100 \mu\text{g m}^{-3}$ or more
27 in the corresponding thermograms. These two constraints resulted in the choice of the
28 0.1, 1 and $10 \mu\text{g m}^{-3}$ bins. Please note that the $0.1 \mu\text{g m}^{-3}$ also includes material with even
29 lower volatility that did not evaporate at the highest temperature used. These important
30 points have been added to revised paper.

31
32 The Karnezi et al. (2014) approach searches the full parameter space for solutions that are
33 consistent (within a predetermined error consistent with the experimental uncertainty)
34 with the measured thermograms. It usually finds a number of such solutions. It then
35 calculates a weighted average (the closer a solution is to the data the higher its weight)
36 and a weighted standard deviation using all these "acceptable" solutions. This brief
37 explanation is now included in the paper.

38
39 **Minor comments**

40
41 **(3) Line 63. Please give the full name of PMF.**
42 It has been added.

43
44 **(4) Line 87 and 88. The sentence reads odd.**
45 We have rephrased the sentence.
46

47 **(5) Line 130. Can the authors briefly describe these two papers?**
48 We have added a short description of these two papers. Xu et al. (2015a) estimated the
49 contribution of different sources to the measured OA while Cerully et al. (2015)
50 quantified the OA hygroscopicity. These two papers use the same AMS dataset with the
51 present study.
52

53 **(6) Line 265. Why no measurements above 100 Celsius?**
54 The experimental set-up used was rather complex because there were four lines (ambient
55 bypass, ambient TD, PILIS bypass, and PILS TD) used in an effort to characterize both
56 the volatility and hygroscopicity of the OA. Because of the multiple objectives of the
57 measurements, the number of temperature steps that could be used in the TD was limited
58 and an upper temperature of 100 C was selected in the design phase of campaign. In
59 retrospect, an even higher temperature would have provided very useful information. We
60 have added a sentence in the Conclusions recommending the use of higher temperatures
61 in additional steps in future studies in that area.
62

63 **(7) Line 367 and 368. This sentence reads odd too.**
64 We have rephrased the sentence.
65

66 **(8) Line 380. “Evaporation coefficient”, do you mean “accommodation coefficient”?**
67 We have rephrased this to “accommodation (evaporation) coefficient” to avoid confusion.
68

69 **(9) Line 399. It should be Figure S6, rather than S7.**
70 Corrected.
71
72

73 **Responses to the Comments of Referee #2**

74
75 (1) The manuscript 'Organic aerosol in the summertime SE US: Components and their
76 link to volatility distribution, oxidation and hygroscopicity' by Kostenidou reports on
77 ambient aerosol measurements using a HR-TOF-AMS coupled to a thermodenuder inlet.
78 Total submicron non-refractory OA was split into four main factors: BBOA, Isoprene-
79 OA, MO-OOA and LO-OOA. The observed thermogram profiles of OA and of each of
80 its four factors are shown, along with the modeled volatility distribution of the
81 components of the sum and the four factors. Lastly, an attempt to reconcile
82 hygroscopicity, O:C and volatility is made. The results presented will make an important
83 contribution to the existing body of knowledge on the composition of OA, specifically,
84 the OA present in a moderately-polluted biogenic-rich region of the SEUS. One potential
85 issue needs to be addressed, and a few other clarifications need to be made for this work
86 to be published.

87 Our responses to the comments of the referee and the corresponding changes to the paper
88 can be found below.

89
90 (2) An interesting observation using this TD-AMS setup from SOAS was that the MO-
91 OOA exhibited a lower MFR subsequent to heating compared to the LO-OOA
92 component of OA. That is, more of the 'more oxygenated' component had evaporated or
93 been destroyed by heating relative to the 'less oxygenated' component. A more detailed
94 explanation for this phenomenon than what is currently provided (essentially referencing
95 the work of Karnezi et al.) is needed. How does the model predict that MO-OOA was
96 composed of less volatile material compared to those of LO-OOA? What observation or
97 information was fed into the Karnezi model, etc.? For instance, MO-OOA and Isoprene-
98 OA appear to exhibit distinct MFR thermogram profiles (figure 2), which the Karnezi
99 model is able to reproduce well. Yet, MO-OOA and Isoprene-OA possess nearly
100 indistinguishable C* versus mass fraction distributions (figure 3). How is the model able
101 to come up with essentially the same composition for two OA factors that exhibit distinct
102 thermogram profiles? One conclusion the authors draw from this MO vs LO thermogram
103 observation is that MFR alone can be misleading. So I assume the authors relied on the
104 model to be the arbiter. What exactly was the contribution of TD?

105 This is an excellent point. It has often been assumed that a lower MFR means more
106 volatile OA and vice versa. This is correct, but it applies to the temperature of the
107 measurement. The volatility of an OA component at a given temperature in the TD
108 depends not only on its volatility at ambient conditions (the ones that we are interested
109 in), but also at its enthalpy of vaporization. A high enthalpy of vaporization leads to
110 drastic increases of the volatility as the temperature increases. The enthalpy of
111 vaporization does affect significantly the slope of the thermogram over the full
112 temperature range. The Karnezi et al. algorithm looks at all potential explanations for the
113 observed behavior and it reports them. These results are shown in Figure 3. The model
114 finds that the observed behavior of the thermograms is probably due to differences in the
115 effective enthalpy of vaporization (higher value for the MO-OOA than for the LO-OOA).
116 This difference appears to be robust considering the estimated uncertainties (Fig. 3e). The
117 model uses the observed MFR, the concentration of each factor, and the size of the
118 particles as inputs for its analysis. We have added the above discussion in the paper.

119

120 The estimated effective enthalpy of vaporization also explains the similarity of the
121 estimated volatility distributions of MO-OOA and Isoprene-OA. However, in this case
122 please note the significant uncertainties of especially the Isoprene-OA volatility
123 distribution for all bins. There are solutions for which for example the MO-OOA is a lot
124 less volatile than the Isoprene-OA. So the measurements in this case are not sufficient to
125 compare the volatilities of the two factors. This is the reason that we did our best in the
126 paper to avoid strong conclusions about comparisons of the volatilities of the various
127 factors. This is now stressed in the Conclusions of the paper.

128

129 Indeed, the model was the arbiter for the analysis. However, the model was constrained
130 by the TD measurements as well as the other measured inputs (OA and factor
131 concentrations determined by the AMS, size distributions, etc.).

132

133 **(3) Are you able to calculate a C^* versus mass fraction distribution at each thermogram**
134 **temperature setting? Determining how the C^* of the material that compose a given OA**
135 **factor evolves as it is incrementally heated would provide an important constraint.**

136 This is a good suggestion. We added the predicted composition in terms of C^* of each
137 factor after passing through the thermodenuder as a function of temperature. We have
138 added a new graph to Figure 1 for the composition of the total OA and we have also
139 added a new figure (Figure 4 in the revised paper) for the composition of the four factors.
140 The model predicts, as expected, that the less volatile material with $C^*=0.1 \mu\text{g m}^{-3}$
141 dominates the composition of the remaining aerosol after the TD as the temperature
142 increases for all factors. However, there are significant differences in the evolution of the
143 composition of the various factors. A short discussion has been added together the new
144 figures.

145

146 **(4) Comparison to previous work on OA measured during SOAS needs to be more**
147 **focused. A thorough comparison (and explanation of why there seems to be a**
148 **discrepancy) to the work of Hu et al. is more appropriate here as the two utilized the same**
149 **approach (TD-AMS). For instance, how do the factor assignment (BBOA, Isoprene-OA,**
150 **MO-OOA, LO-OOA) compare to that of the Jimenez group? That data is publicly**
151 **available and comparison to it should be included in the analysis. In comparing against**
152 **the works of Saha and Lopez-Hilfiker, a discussion of how different techniques can yield**
153 **different observations or interpretations is more suitable. For instance, the thermogram**
154 **profiles obtained from shown by Lopez-Hilfiker et al. show residual IEPOX signal**
155 **desorbing off the FIGAREO-CIMS inlet well above 100C whereas the TD-AMS saw**
156 **none above 100C. Suggesting artifact in another method without supporting evidence is**
157 **not justified.**

158 Hu et al. (2016) also used a thermodenuder in order to estimate the Isoprene-OA and the
159 total OA volatility distribution. Even though they used practically the same measurement
160 technique as we did, their approach for the measurement interpretation was very different.

161 Hu et al. (2016) used the empirical method of Faulhaber et al. (2009) and not an aerosol
162 dynamics model for the estimation of the volatility distributions from their MFR
163 measurements. Their method is based on a relationship between TD temperature and
164 organic species saturation concentration at 298 K (C^*) that has been obtained using 5

165 compounds (acids) with known saturation concentration. This approach is applicable to
166 organic compounds with similar properties (e.g., enthalpy of vaporization) to the 5
167 known compounds, but it may encounter significant difficulties for OA that is quite
168 different from the model compounds. A related weakness of that approach is that it does
169 not account for the enthalpy of vaporization as the model used in this work does. We
170 have added this discussion in the text.

171
172 Hu et al. (2016) (if this is the paper that the reviewer is referring as Jimenez et al. group)
173 presented results only for the IEPOX-OA and total OA. These results are compared to
174 ours in Figure S6.

175
176 Please note that the Lopez-Hilfiker et al. (2016) results, as explained in the text (lines
177 418-430 of the original manuscript), are strictly for the IEPOX SOA which is a subset of
178 the Isoprene-OA investigated here. So a quantitative comparison of the corresponding
179 volatilities is not possible. Also, the analysis of Lopez-Hilfiker et al. (2016) does not
180 account for the effect of the vaporization enthalpy. There is of course a potentially
181 important experimental difference in this case, as in our work the OA just evaporates in
182 the TD, while the Lopez-Hilfiker et al. (2016) experimental approach involves collection
183 of the OA on a filter and then heating and desorption. We have added additional
184 discussion of these differences to the revised paper.

185
186 Saha et al. (2017) obtained the total OA thermogram using a thermogravimetric system and
187 then estimated the corresponding volatility distribution using an aerosol dynamics model
188 and the volatility basis set (Donahue et al., 2006; Lee et al., 2011; Saha et al., 2015; Saha
189 and Grieshop, 2016). Their experimental and data analysis approach is a lot closer to ours
190 compared to Hu et al. (2016) and Lopez-Hilfiker et al. (2016) and their results for the
191 total OA are quite consistent with ours. Their model takes into account the vaporization
192 enthalpy as well and this is probably the key difference among the various approaches.
193 This issue is now discussed in more detail in the paper.

194
195 **(5) Why do the abundance distributions predicted for the OA factors (Figure 3a-3d) look**
196 **the way they do? That is, why do those for MO-OOA, LO-OOA and isoprene-OA appear**
197 **to be bi-modal, whereas that of BBOA is not? Perhaps it is this arbitrary designation into**
198 **three log base-10 bins that obscures the real distribution? Can the distributions be shown**
199 **on finer C* scales? What is the lower limit of C* that can be detected with this approach?**
200 **But basically, what is the source of the low volatility material as opposed to the high**
201 **volatility material? OH versus O₃ versus NO₃? Aging? Is there an atmospheric chemistry**
202 **explanation for the calculated volatility distribution?**

203 The selection of the three volatility bins was not arbitrary, but was based on the ambient
204 measured concentration and the available TD data (the number of selected temperatures).
205 This issue is also discussed in our response to Comment 2 of Referee 1. One can use
206 additional bins in the fitting algorithm either extending the range or providing additional
207 resolution, but the results will be meaningless (e.g., fitting four measurements with a
208 model using five or more parameters). With only three volatility bins and the
209 corresponding uncertainties a more detailed analysis of the shape of the distributions will
210 not add much to the paper.

211
212 In theory, the TD approach can go down to concentrations as low as 10^{-5} $\mu\text{g m}^{-3}$ or even
213 lower if a high enough temperature is used. For example, Louvaris et al. (2017) used
214 temperatures up to 400°C. Of course, the major problem is that use of higher
215 temperatures may lead to a series of reactions in the aerosol phase (fragmentation, etc.)
216 introducing considerable uncertainty in the corresponding measurements. The
217 temperature and corresponding volatility range used in this study are considered
218 relatively “safe” even if artifacts due to reactions are still expected even in this relatively
219 low temperature range. We have added a few sentences explaining this point.

220
221 The AMS cannot provide detailed information about the identity of the compounds in
222 each volatility bin. Use of other chemical analysis techniques is required and would be
223 extremely helpful in linking the volatility distribution with atmospheric processes. This is
224 now mentioned in the Conclusions section.

225
226 **(6) The error bars shown in Figures 1 and 2 indicate there is little variability in the**
227 **thermogram profiles throughout the SOAS campaign. Have the authors looked for any**
228 **dependence of the steepness of the thermogram profiles on time of day, high/low OA**
229 **loading, RH, temperature, particle acidity, high/low NO_x, etc., all of which varied widely**
230 **through the duration of SOAS?**

231 We have followed the suggestion of the reviewer and examined the correlation between
232 the MFR of each factor at each temperature with the RH, temperature, O₃, NO, NO₂,
233 acidity and OA loading. In addition, we checked the diurnal profiles of each factor at
234 each temperature.

235
236 There was a tendency of the MFR of all factors at higher temperatures to increase as the
237 ozone concentration increased. For example, the R² between O₃ and the MFR of MO-
238 OOA at 80°C was 0.25, R²=0.36 for the MFR of LO-OOA at 100°C, R²=0.26 for the
239 MFR of Isoprene OA at 100°C and R²=0.22 for the MFR of BBOA at 100°C. This
240 suggests that when the photochemistry is more intense the OA evaporates less in the TD.
241 The R² between the acidity and the MFR of LO-OOA at 100°C was 0.26, suggesting that
242 acidity may be also affecting the MFR. The MFR of BBOA at 100°C on the other hand
243 was anti-correlated to the NO and NO₂ concentrations (R² of 0.23 and 0.37
244 correspondingly). This indicates that at lower NO_x levels (away from the source) BBOA
245 evaporated less, suggesting that this factor may contain both fresh and aged BBOA or
246 fresh BBOA aerosols mixed with aged background. This is also supported by the
247 relatively high O:C ratio of this factor (0.58). All the other R² values examined were
248 lower than 0.2.

249
250 There was no distinct diurnal profile for the MO-OOA, BBOA and Isoprene-OA MFR.
251 For LO-OOA MFR at 80°C and 100°C there was a slight increase (with a lot of noise
252 though) between 11:00-16:00. As a result, we do not have much evidence to support a
253 significant diurnal variation of the MFR of the various factors.

254
255 We have added a paragraph in the manuscript describing the above results.
256

257 (7) A strong point was made that the findings of Jimenez et al. (2009) had been
258 contradicted, but no thorough explanation for the possible reason for the discrepancy.

259 Our conclusion is that the proposed relationship of Jimenez et al. (2009) does not apply to
260 all environments and especially when multiple aerosol sources and types are present. One
261 possible reason may be that the O:C-hygroscopicity relationship may not be monotonic,
262 but there may be systems for which the relationship may be highly nonlinear. For
263 example, Cain and Pandis (2017) showed that the hygroscopicity could exhibit a
264 maximum at intermediate volatilities. This suggests that the relationship between the
265 hygroscopicity and the volatility may also be highly nonlinear. We have added a few
266 sentences in the Conclusions discussing this point.

267
268 (8) References made in some of the SI figures are not in the SI citation list.

269 We have added the citations to the work of Karnezzi et al. (2014), Nakao et al. (2017),
270 Ulbrich et al. (2009) and Xu et al. (2015).

271
272

273 **Organic aerosol in the summertime Southeastern United States: Components and**
274 **their link to volatility distribution, oxidation state and hygroscopicity**

275

276 Evangelia Kostenidou^{1,2}, Eleni Karnezi³, James R. Hite Jr⁴, Aikaterini Bougiatioti^{4,6}, Kate
277 Cerully^{5a}, Lu Xu^{5,b}, Nga L. Ng^{5,4}, Athanasios Nenes^{1,4,5,6*} and Spyros N. Pandis^{1,2,3*}

278

279 ¹Institute of Chemical Engineering Sciences, Foundation for Research and Technology,
280 Hellas, Patras, Greece

281 ²Department of Chemical Engineering, University of Patras, Patras, Greece

282 ³Department of Chemical Engineering, Carnegie Mellon University, Pittsburgh, USA

283 ⁴School of Earth and Atmospheric Sciences, Georgia Institute of Technology, Atlanta,
284 GA, USA

285 ⁵School of Chemical and Biomolecular Engineering, Georgia Institute of Technology,
286 Atlanta, GA, USA

287 ⁶Institute for Environmental Research and Sustainable Development, National
288 Observatory of Athens, Palea Penteli, Greece

289 ^anow at: TSI, Inc., Shoreview, MN, USA

290 ^bnow at: Division of Geological and Planetary Sciences, California Institute of
291 Technology, Pasadena, CA, USA

292

293 *correspondence to athanasios.nenes@gatech.edu, spyros@chemeng.upatras.gr

294

295 **Abstract**

296 The volatility distribution of the organic aerosol (OA) and its sources during the Southern
297 Oxidant and Aerosol Study (SOAS; Centerville, Alabama) was constrained using
298 measurements from an Aerodyne High-Resolution Time-of-Flight Aerosol Mass
299 Spectrometer (HR-ToF-AMS) and a thermodenuder. Positive Matrix Factorization (PMF)
300 analysis was applied on both the ambient and thermodenuded high resolution mass
301 spectra, leading to four factors: more oxidized oxygenated OA (MO-OOA), less oxidized
302 oxygenated OA (LO-OOA), an isoprene epoxydiols (IEPOX) related factor (Isoprene-
303 OA) and biomass burning OA (BBOA). BBOA had the highest mass fraction remaining

304 (MFR) at 100°C, followed by the isoprene-OA, and the LO-OOA. Surprisingly the MO-
305 OOA evaporated the most in the TD. The estimated effective vaporization enthalpies
306 assuming an evaporation coefficient equal to unity were 58 ± 13 kJ mol⁻¹ for the LO-OOA,
307 89 ± 10 kJ mol⁻¹ for the MO-OOA, 55 ± 11 kJ mol⁻¹ for the BBOA, and 63 ± 15 kJ mol⁻¹ for
308 the Isoprene-OA. The estimated volatility distribution of all factors covered a wide range
309 including both semi-volatile and low-volatility components. BBOA had the lowest
310 average volatility of all factors, even though it had the lowest O:C ratio among all factors.
311 LO-OOA was the more volatile factor and its high MFR was due [according to the model](#)
312 to its low enthalpy of vaporization [according to the model](#). The Isoprene-OA factor had
313 intermediate volatility, quite higher than suggested by a few other studies. The analysis
314 suggests that deducing the volatility of a factor only from its MFR could lead to
315 erroneous conclusions. The oxygen content of the factors can be combined with their
316 estimated volatility and hygroscopicity to provide a better view of their physical
317 properties.

318

319 1. Introduction

320 Population exposure to atmospheric particulate matter (PM) increases premature
321 mortality from cardiovascular and respiratory diseases (Pope et al., 2002; IARC, 2013;
322 Cohen et al., 2017). The same particles also modulate the planetary radiative balance and
323 hydrological cycle (IPCC, 2013; NASEM, 2016; Seinfeld et al., 2016). Organic aerosol
324 (OA) constitutes a significant part of submicron aerosol mass (Zhang et al., 2007) and it
325 is characterized by daunting chemical complexity (Kanakidou et al., 2005; Hallquist et al.,
326 2009). OA is directly emitted from anthropogenic and natural sources, but it is also
327 produced by condensation of products formed during the oxidation of gas-phase organic
328 compounds with O₃, NO₃ and OH radicals (secondary organic aerosol, SOA; Kanakidou
329 et al., 2005). OA formation can be further promoted by the interactions of anthropogenic
330 and biogenic compounds; in the southeastern United States, anthropogenic sulfate
331 enhances OA formation through rapid reactive uptake of IEPOX to particles and aqueous
332 phase reactions (Xu et al., 2015a; Xu et al., 2016a; Budisulistiorini et al., 2017).

333 Several approaches have been developed to unravel the sources and the degree of
334 atmospheric processing of aerosol sampled by the AMS. These include custom principal

335 component analysis (Zhang et al., 2005), multiple component analysis (Zhang et al.,
336 2007), [Positive Matrix Factorization \(PMF\)](#) (Paatero and Tapper 1994; Lanz et
337 al., 2007) and the multilinear engine (ME-2) (Lanz et al., 2008; Canonaco et al., 2013).
338 Applying the above source apportionment techniques on AMS mass spectra, information
339 about the aerosol sources and the degree of the atmospheric processing can be derived.
340 Important primary components include hydrocarbon-like OA (HOA) (Zhang et al., 2005)
341 and biomass burning OA (BBOA) (Aiken et al., 2009). The most abundant and
342 ubiquitous OA component is the oxygenated OA (OOA), which often consists of a more
343 oxygenated (MO-OOA) and a less oxygenated OA (LO-OOA) factor (Lanz et al., 2007).
344 In the southeastern (SE) United States, MO-OOA and LO-OOA are dominant factors,
345 comprising 47-79% of the total OA (Xu et al., 2015b). Factors related to biogenic
346 secondary OA have been identified in urban, suburban and remote areas (Budisulistiorini
347 et al., 2013; Chen et al., 2015; Kostenidou et al., 2015). In the SE United States, an
348 Isoprene-OA factor linked to IEPOX uptake is present during warm periods, contributing
349 up to 36% of the total OA in the summertime (Xu et al., 2015b).

350 Central to understanding the atmospheric impacts of OA is constraining its
351 volatility and hygroscopicity (Kanakidou et al., 2005). Volatility measurements are mostly
352 carried out using heated laminar flow reactors, known as thermodenuders (TD)
353 (Burtscher et al., 2001; An et al., 2007) or isothermal dilution (Grieshop et al., 2009). In
354 these systems, changes in OA mass concentration are related to the OA evaporation rate
355 and its volatility can be estimated. The comparison of aerosol evaporation measurements
356 across studies and conditions with TD or isothermal dilution chambers is not
357 straightforward. The established proxy for volatility is the “mass fraction remaining
358 (MFR)”, i.e., the mass of the aerosol remaining after a volatility measurement (Huffman
359 2009; Cerully et al., 2015; Xu et al., 2016b). MFR has often been used as a relative
360 measure of volatility, ~~as it is assumed that the volatility of particulate matter increases as~~
361 ~~MFR decreases for particles and TD conditions that are otherwise identical as it is~~
362 ~~assumed that the volatility of particulate matter increases as MFR decreases for similar~~
363 ~~particle sizes and TD operation conditions.~~ Although clearly linked to volatility, the
364 MFR depends on the enthalpy of vaporization (ΔH_{vap}), the aerosol concentration, the
365 heating section residence time, the particle size distribution, and potential particle-to-gas

366 mass transfer resistances. All these parameters therefore complicate the linking of the
367 measured MFR to the volatility. An additional complication is that organic aerosol
368 mixtures are characterized by a distribution of volatilities. A number of studies have
369 attempted to estimate this volatility distribution with appropriate TD models (Cappa and
370 Jimenez, 2010; Lee et al., 2010; Paciga et al., 2016; Saha and Grieshop 2016; Louvaris et
371 al., 2017; Saha et al., 2017).

372 Three studies have reported volatility distributions of the isoprene (or IEPOX)
373 SOA and the total OA for the southeastern United States. Lopez-Hilfiker et al. (2016)
374 suggested that the IEPOX SOA had a very low saturation concentration with $C^*=10^{-4}$ μg
375 m^{-3} , based on the FIGAERO-CIMS signals of $\text{C}_5\text{H}_{12}\text{O}_4$ and $\text{C}_5\text{H}_{10}\text{O}_3$. They assumed that
376 these signals correspond to 2-methyltetrols and 3-MeTHF-3,4-diols and/or C5 alkene
377 triols, which are tracers for isoprene SOA. Using the total FIGAERO-CIMS signal
378 ($\text{C}_x\text{H}_y\text{O}_z\text{N}_{0-1}$) the same authors estimated an extremely low total OA average volatility of
379 $C^*=3.7\times 10^{-7}$ μg m^{-3} for the OA with ELVOCs representing 99% of the total OA. This is
380 the lowest reported volatility for ambient OA in the literature. Hu et al. (2016) estimated
381 an average volatility of $C^*=5.2\times 10^{-5}$ μg m^{-3} for the IEPOX SOA. Their results were based
382 on the MFR of the IEPOX SOA (calculated by PMF) using ambient and thermodenuded
383 AMS measurements. The volatility distribution of IEPOX SOA was estimated applying
384 the technique of Faulhaber et al. (2009). The corresponding total OA volatility
385 distribution covered the range from $C^*=10^{-9}$ to 1 μg m^{-3} . Saha et al. (2017) used an
386 Aerosol Chemical Speciation Monitor (ACSM) and a thermodenuder to estimate an
387 average total OA volatility of $C^*=0.21$ μg m^{-3} and a vaporization enthalpy of 100 kJ mol^{-1} .

388 The two-dimensional volatility basis set (2D-VBS) framework, describing the
389 OA concentration as a function of its oxygen content and volatility is a promising
390 approach to describe the partitioning and chemical evolution of the thousands of
391 compounds present in OA (Donahue et al., 2012). If expanded to include hygroscopicity,
392 the framework can be strengthened considerably. Several studies have attempted to link
393 hygroscopicity and volatility (Kuwata et al., 2007; Asa-Awuku et al., 2009; Frosh et al.,
394 2013) or hygroscopicity and oxidation state (Masoli et al., 2010; Chang et al., 2010;
395 Lathem et al., 2013; Thalman et al., 2017), however only a few focus on all the properties
396 combined (Jimenez et al., 2009; Tritscher et al., 2011; Cerully et al., 2015). Jimenez et al.

397 (2009) combined data from various studies and suggested that hygroscopicity and
398 oxidation state increase as volatility decreases. The generality of this finding has been
399 questioned by subsequent studies (Meyer et al., 2009; Tritscher et al., 2011; Lathem et al.,
400 2013). Recently, Nakao (2017) proposed a theoretical framework, in which the
401 hygroscopicity is explicitly related to oxidation state and volatility. With this approach,
402 each OA “source” can have a unique set of volatility and hygroscopicity parameters that
403 evolve with atmospheric oxidative aging – along a path that requires further constraints
404 from chemistry.

405 ~~In this study we build upon the work of Xu et al. (2015a) and Cerully et al. (2015)~~
406 ~~and attempt to constrain the volatility distributions and effective vaporization enthalpy of~~
407 ~~each PMF factor of OA sampled during the SOAS field campaign at Centreville,~~
408 ~~Alabama. In this study we build upon the work of Xu et al. (2015a) and Cerully et al.~~
409 ~~(2015). Xu et al. (2015a) estimated the contribution of the different sources to the~~
410 ~~measured OA, while Cerully et al. (2015) quantified the OA hygroscopicity during the~~
411 ~~SOAS field campaign at Centreville, Alabama. In this work we build upon these studies~~
412 ~~and attempt to constrain the volatility distributions and effective vaporization enthalpy of~~
413 ~~each PMF factor of OA sampled during the same field campaign.~~ We then proceed to
414 associate the hygroscopicity parameters estimated by Cerully et al. (2015) with the
415 volatility distributions and test their consistency with the Nakao (2017) theoretical
416 framework.

417

418 2. Experimental

419 2.1 Measurement site and campaign

420 The measurements were performed in Centreville, Alabama, (32°54'11.81"N,
421 87°14'59"W). The station was located in an area significantly influenced by biogenic
422 emissions (Liao et al., 2007; Spracklen et al., 2011). Anthropogenic emissions also affect
423 the site. The measurements were conducted during the Southern Oxidant and Aerosol
424 Study (SOAS), which was part of the Southern Atmosphere Study (SAS;
425 <http://www.eol.ucar.edu/projects/sas>) from June 1 to July 15 2013. A summary of
426 important findings can be found in Carleton et al. (2017), while additional results relevant

427 ~~tofer~~ our study can be found in Xu et al. (2015a), Cerully et al. (2015), Guo et al. (2015)
428 and Saha et al. (2017).

429

430 **2.2 Instrumentation**

431 The aim of the specific measurements was to characterize both the ambient and
432 the water soluble fraction of the non-thermally and thermally-denuded PM₁. For the
433 vaporization a thermodenuder, TD, (Cerully et al., 2014) was used. A particle-into-liquid
434 sampler (PILS) (Weber et al., 2001) was used to collect the water soluble aerosol
435 components and then the solution was nebulized. The aerosol passed every 12 or 15 min
436 through four lines: ambient bypass, ambient TD, PILS bypass and PILS TD. In this work
437 we used the ambient denuded measurements only. Details about the experimental set up
438 can be found in Cerully et al. (2015).

439 The sampling instrumentation included an Aerodyne HR-AMS, a Scanning
440 Mobility Particle Sizer (SMPS, Classifier model 3080, DMA model 3081, CPC model
441 3022A, TSI) ~~and~~, a Cloud Condensation Nuclei counter (CCNc, Droplet Measurement
442 Technologies). The TD used in this campaign has been characterized by Cerully et al.
443 (2014). Briefly, the TD consisted of a heating and a cooling section. The first part was a
444 stainless steel tube ~~of 30-with~~ in length and 0.68 in inner diameter. The cooling section
445 was removed during this campaign, as the re-condensation of the vapors is minimal when
446 the ambient mass concentration is low, which was the case for this campaign (Cappa et
447 al., 2010; Saleh et al., 2011; Cerully et al., 2014). The temperature in the TD was 60, 80
448 and 100°C. The total flow rate passing through the TD was 1.5 L min⁻¹ and so the average
449 TD residence time was approximately 7 s.

450

451 **3. Data Analysis**

452 **3.1 PMF and elemental ratios**

453 PMF (Lanz et al., 2007) was applied to both ambient bypass and TD HR organic
454 mass spectra according to the procedure of Ulbrich et al. (2009). Details about the PMF
455 solution are provided in the SI (Figures S1 and S2). The O:C and H:C elemental ratios
456 were estimated using the approach of Canagaratna et al. (2015). Xu et al. (2015a) also
457 used the Canagaratna et al. (2015) O:C approach, however Cerully et al. (2015) applied

458 the older algorithm of Aiken et al. (2008). For any comparisons between this work and
459 previous studies we converted the old O:C to the new O:C ratios using the corresponding
460 f_{44} fraction according to the equation: $O:C=0.079+4.31 f_{44}$ (Canagaratna et al., 2015).

461

462 **3.2 Collection efficiency (CE)**

463 Xu et al. (2015a) estimated the AMS CE using the composition-dependent
464 approach of Middlebrook et al. (2012). The average bypass CE was estimated to be
465 0.65 ± 0.12 , while the average TD CE was slightly higher 0.7 ± 0.11 . The difference was
466 statistically significant with a p value less than 0.0001. These estimates can be more
467 uncertain than their variability suggests, due to their sensitivity to aerosol ammonium and
468 neutralization. The sensitivity of our results is discussed in Section 5.3.

469

470 **3.3 TD losses**

471 The thermodenuded OA was corrected for particle losses due to sedimentation,
472 diffusion and thermophoresis inside the thermodenuder. More details about the
473 thermodenuder characterization are provided by Cerully et al. (2014).

474

475 **3.4 MFR**

476 For the MFR calculations only data with ambient OA concentration higher than
477 $0.2 \mu\text{g m}^{-3}$ were used in order to avoid extreme variations of the MFR. For such low
478 concentrations the corresponding TD concentrations can be very low introducing
479 significant error in the MFR calculation. The fractions of the data for each factor above
480 the threshold of $0.2 \mu\text{g m}^{-3}$ are given in Table 1. For the total OA, MO-OOA and LO-
481 OOA this fraction was above 92% but for the Isoprene-OA and BBOA was lower (76%
482 and 42% respectively). The four (or five) consecutive ambient and TD measurements
483 during each hour were averaged. The variability of the four (or five) averaged values was
484 4-16%.

485

486 **3.5 Volatility distribution estimation**

487 The dynamic mass transfer model of Riipinen et al. (2010) was used to estimate the OA
488 volatility distributions. The model simulates the particle evaporation inside the

489 thermodeuder solving the corresponding system of differential equations describing the
 490 mass transfer between the particle and gas phases:

$$491 \quad \frac{dm_p}{dt} = -\sum_{i=1}^n I_i \quad (1)$$

$$492 \quad \frac{dC_i}{dt} = I_i N_{tot} \quad (2)$$

493 where m_p is the organic particle mass, C_i is the gas-phase concentration of compound i ,
 494 N_{tot} is the total number concentration of the particles, n is the number of the assumed
 495 organic aerosol components, and I_i the mass flux of the compound i given by the Vesala
 496 et al. (1997) equation:

$$497 \quad I_i = \frac{2\pi d_p \rho M_i D_i \beta_{mi}}{RT_{TD}} \ln \left[\frac{1 - \frac{p_i}{p}}{1 - \frac{p_i^0}{p}} \right] \quad (3)$$

498 where d_p is the particle diameter, R the molar gas constant, M_i and D_i the molar mass and
 499 the diffusion coefficient of compound i at temperature T_{TD} . The diffusion coefficient (D_i)
 500 depends on the temperature and is calculated according to Chen and Othmer (1962) and
 501 β_{mi} is the correction factor given by Fuchs and Sutugin (1970). p is the total gas pressure,
 502 while p_i and p_i^0 are the partial vapor pressures of the compound i at the particle surface
 503 and far away from the particle respectively. p_i^0 is given by:

$$504 \quad p_i^0 = x_i \gamma_i p_{sat,i} \exp\left(\frac{4M_i \sigma}{RT_p \rho d_p}\right) = x_{mi} \frac{C_i^* RT_{TD}}{M_i} \exp\left(\frac{4M_i \sigma}{RT_p \rho d_p}\right) \quad (4)$$

505 where x_i is the mole fraction of i , γ_i the activity coefficient of i in the particle, $p_{sat,i}$ the
 506 pure component vapor pressure of i over a flat surface, T_p the particle temperature (we
 507 assume that $T_p = T_{TD}$), x_{mi} the mass fraction of i in the particle, ρ the particle density and σ
 508 the particle surface tension. C_i^* is the effective saturation concentration of i at 298 K.

509 The change of the vapor pressure with temperature is calculated by the Clausius-
 510 Clapeyron equation:

$$511 \quad C_i^*(T_{TD}) = C_i^*(298 K) \exp\left[\frac{\Delta H_{vap,i}}{R} \left(\frac{1}{298} - \frac{1}{T_{TD}}\right)\right] \frac{298}{T_{TD}} \quad (5)$$

512 where ΔH_{vap} is the vaporization enthalpy of component i .

Field Code Changed

Field Code Changed

Field Code Changed

Formatted: Font: Italic

Formatted: Font: Italic

Field Code Changed

Formatted: Font: Italic

Formatted: Font: Italic

Formatted: Font: Italic

Formatted: Font: Italic

Formatted: Font: Italic

Field Code Changed

Formatted: Font: Italic

513 The model inputs include the loss-corrected MFRs, the thermodenuder
514 temperature and residence time, the bypass average particle size, and the average ambient
515 OA concentration and the aerosol density (which was assumed 1.4 g cm^{-3} for all cases).
516 The output of the model is the OA volatility distribution in terms of effective saturation
517 concentrations (C^*) at 298 K, in combination with its effective vaporization enthalpy
518 (ΔH_{vap}) and the mass accommodation (evaporation) coefficient (a_m). We fit the measured
519 thermograms using a consecutive 3-bin C^* distribution, with varying mass fraction in
520 each bin. The bins corresponded to saturation concentrations of 0.1, 1, and $10 \mu\text{g m}^{-3}$ at
521 298 K. The enthalpy of vaporization (ΔH_{vap}) was also estimated, while the
522 accommodation coefficient was assumed to be equal to unity. The best (optimum)
523 solutions and the corresponding uncertainties are calculated using the approach algorithm
524 of Karnezi et al. (2014). The Karnezi et al. (2014) approach searches the full parameter
525 space for solutions that are consistent (within a predetermined error consistent with the
526 experimental uncertainty) with the measured thermograms, within a predetermined error
527 consistent with the experimental uncertainty. The algorithm approach usually finds a
528 number of such solutions. It then calculates a weighted average (the closer a solution is to
529 the data the higher its weight) and a weighted standard deviation using all these
530 “acceptable” solutions. For each solution the average mass fraction in each bin and its
531 corresponding standard deviation, was estimated using the top 2% of the mass fraction
532 combinations with the lowest error. In this study for the comparison between volatilities
533 we will also use the average volatility based on mass fraction weighted $\log_{10} C^*$.

Formatted: Font color: Auto

Formatted: Font color: Auto

Formatted: Font: Italic

Formatted: Font: Italic

Formatted: Font: Italic

Formatted: Font: Italic

535 3.6 Hygroscopicity

536 ~~Details about the hygroscopicity analysis of the corresponding data can be found~~
537 ~~in Cerully et al. (2015).~~ Using a CCN counter Cerully et al. (2015) estimated the
538 hygroscopicity parameter κ of the total and water soluble ambient and thermodenuded
539 PM_{10} OA. The same authors performed linear regression of the ambient water soluble κ_{org}
540 with the PMF factors of the ambient water soluble OA. During the periods of the water
541 solubility measurements the BBOA concentration was too low to allow the separation of
542 the factor, so its hygroscopicity was not determined. The PMF results of the ambient total

543 and the ambient water soluble data were practically the same. [Additional details about the](#)
544 [hygroscopicity analysis can be found in Cerully et al. \(2015\).](#)

545

546 4. Results and Discussion

547 4.1 Volatility of organic aerosol

548 The average OA mass concentration was $5 \mu\text{g m}^{-3}$. The loss-corrected OA MFR is
549 depicted in Figure 1a.– Half of the total OA evaporated at 100°C ($T_{50}=100^\circ\text{C}$). The
550 estimated volatility distribution (Figure 1b) indicates that 46% of the organic aerosol was
551 semivolatile organic compounds (SVOCs) (compounds with $1 \leq C^* \leq 100 \mu\text{g m}^{-3}$) and
552 54% was low volatility organic compounds (LVOCs) ($0.001 \leq C^* \leq 0.1 \mu\text{g m}^{-3}$). Part of
553 the material assigned to the $0.1 \mu\text{g m}^{-3}$ bin has volatility less than this value. The fact that
554 there were no measurements above 100°C does not allow us to constrain further the
555 contributions of the LVOCs and ELVOCs. [The number of bins that can be used in the](#)
556 [analysis of thermodenuder data is in general determined by the ambient OA concentration](#)
557 [\(the bin range can extend up to an order of magnitude higher than the measured values\),](#)
558 [the number of temperature steps used in the analysis \(the number of bins cannot be ~~much~~](#)
559 [higher than the number of data points available for fitting\), and the maximum fraction of](#)
560 [the OA evaporated during the analysis. In theory, the thermodenuder approach can go](#)
561 [down to concentrations as low as \$10^{-5} \mu\text{g m}^{-3}\$ or even lower if a high ~~enough~~ temperature](#)
562 [is used. For example, Louvaris et al. \(2017\) used temperatures up to \$400^\circ\text{C}\$.– Our](#)
563 [selection of only 3 bins was determined by \(The availability of measurements at 25, 60,](#)
564 [80 and \$100^\circ\text{C}\$ means a maximum of 4 bins are possible; however, ~~The concentration of~~](#)
565 [since the OA was of the order of \$5 \mu\text{g m}^{-3}\$, so there is a the thermograms contain little](#)
566 [information on the ~~about~~ partitioning of compounds with saturation concentration](#)
567 [of ~~exceeding~~ \$100 \mu\text{g m}^{-3}\$ –or–more–in–the–corresponding–thermograms. These two](#)
568 [constraints together resulted in the choice of ~~the~~ three volatility bins: \$0.1\$, \$1\$ and \$10 \mu\text{g m}^{-3}\$](#)
569 [bins. The average volatility based on mass fraction weighted \$\log_{10}C^*\$ values was](#)
570 $C^*=0.55\pm 0.29 \mu\text{g m}^{-3}$. Please note that this value is useful only for comparisons of
571 volatility distributions in the same VBS volatility range. The mass fraction of each
572 volatility bin is provided in Table S1. The effective vaporization enthalpy of the total OA
573 was $86\pm 9 \text{ kJ mol}^{-1}$.

Formatted: Font: Italic

574

575 4.2 Volatility of OA components

576 The PMF analysis using both the ambient and TD measurements suggested four
577 factors. The OA consisted of 43% more oxidized OOA (MO-OOA), 29% less oxidized
578 OOA (LO-OOA), 19% Isoprene-OA and 9% biomass burning OA (BBOA). The same
579 four factors and OA composition were obtained by Xu et al. (2015a) using only the
580 ambient AMS HR mass spectra (Table 2). Details about their characteristics, correlation
581 with external tracers and justification of their names are provided by Xu et al. (2015a).
582 The ambient OA factor time series were practically the same in the two analyses with
583 $R^2 > 0.93$, the mass spectra were also similar with angle θ equal to 3-4 degrees for LO-
584 OOA, MO-OOA and Isoprene-OA and 12 degrees for the BBOA factor (Figure S3).
585 Thus, our PMF results are robust and quite consistent with the previous analysis.

586 The loss-corrected MFRs of the four factors are depicted in Figure 2. BBOA
587 evaporated less, as its MFR was close to unity at all temperatures. The BBOA factor was
588 quite oxygenated with an O:C of 0.58 compared to previous studies (e.g., Crippa et al.,
589 2013; Florou et al., 2017). The corresponding BBOA could be chemically aged or PMF
590 may be mixing the BBOA with aged background OA. Even though BBOA and Isoprene-
591 OA had similar O:C ratios (0.58 and 0.59 correspondingly), the Isoprene-OA MFR was
592 lower. Surprisingly the MFR of MO-OOA was lower than that of LO-OOA, even though
593 MO-OOA had a higher a O:C ratio (0.99) than LO-OOA (0.63). Relying only on MFR
594 one would reach the conclusion that MO-OOA was more volatile than LO-OOA.

595 The predicted thermograms for each factor are also depicted in Figure 2 and the
596 resulting volatility distributions are shown in Figures 3a-3d. Figures 3e and 3f show the
597 comparison of the volatility compositions and the vaporization enthalpies between the
598 four OA factors. The mass fractions of each volatility bin (in the aerosol phase), average
599 volatility (C^*) and the vaporization enthalpy of each factor are given in Table S1.

600 The average LO-OOA mass concentration was $1.66 \mu\text{g m}^{-3}$ and this factor based
601 on the model was composed of 73% SVOCs and 27% LVOCs. Its average volatility was
602 $C^* = 1.88 \pm 0.32 \mu\text{g m}^{-3}$ and its effective vaporization enthalpy $58 \pm 13 \text{ kJ mol}^{-1}$. The average
603 MO-OOA mass concentration was $1.96 \mu\text{g m}^{-3}$. According to its volatility distribution
604 56% of the MO-OOA was SVOCs and 44% was LVOCs. Its effective vaporization

605 enthalpy was $89 \pm 10 \text{ kJ mol}^{-1}$ and its average volatility $0.95 \pm 0.31 \mu\text{g m}^{-3}$. According at
606 least to the model the MO-OOA was less volatile on average than the LO-OOA even if it
607 evaporated more in the TD. This counterintuitive behavior is explained by the TD model
608 by the higher effective vaporization enthalpy of the MO-OOA, probably due to the
609 contribution of dicarboxylic and tricarboxylic acids which have vaporization enthalpies
610 higher than 100 kJ mol^{-1} (e.g., Saleh et al., 2008; 2010; Kostenidou et al.,
611 [2018submitted](#)). In addition, the C^* distributions as function of the mass fraction and the
612 temperature indicates that as the temperature increases, MO-OOA is composed of a
613 higher fraction of less volatile species ($C^*=0.1 \mu\text{g m}^{-3}$) compared to LO-OOA (Figures 4a
614 and 4b). This ~~enhances~~ supports our finding that the MO-OOA factor contains less
615 volatile species than LO-OOA.

616 Our results suggest that deducing the volatility of a component using only its
617 MFR or its O:C ratio may lead to incorrect conclusions. It has often been assumed that a
618 lower MFR means more volatile OA and vice versa. However, this applies to the
619 temperature of the measurement. The volatility of an OA component at a given
620 temperature in the TD depends not only on its volatility at ambient conditions, but also at
621 its enthalpy of vaporization. A high enthalpy of vaporization leads to drastic increases of
622 the volatility as the temperature increases. ~~The enthalpy of vaporization does and~~
623 substantially affects significantly the slope of the thermogram over the full temperature
624 range. The Karnezi et al. (2014) algorithm looks at all potential explanations for the
625 observed behavior and it reports them. These results are shown in Figure 3. The model
626 finds that the observed behavior of the thermograms is probably ~~due~~ related to differences
627 in the effective enthalpy of vaporization (higher value for the MO-OOA than for the LO-
628 OOA). This difference appears to be robust considering the estimated uncertainties
629 (Figure 3e). In addition, ~~This finding is also supported by~~ Xu et al. (2016b), ~~observed~~
630 contradictions between O:C ratio and MFRs and ~~where~~ they suggested that different O:C
631 distributions could result in the same bulk O:C but different volatility distributions, which
632 may lead to particles with the same O:C but different MFR.

633 BBOA was the less abundant factor with average mass concentration equal to 0.5
634 $\mu\text{g m}^{-3}$. According to the TD model, 53% of the BBOA consisted of SVOCs and the other
635 47% was LVOCs. Its average volatility was $C^*=0.59 \pm 0.22 \mu\text{g m}^{-3}$ and its effective

Formatted: Not Highlight

Formatted: Not Highlight

Formatted: Not Highlight

Formatted: Not Highlight

Formatted: Not Highlight

636 vaporization enthalpy was 55 ± 11 kJ mol⁻¹. The BBOA volatility distribution did not
637 change significantly by the with temperature (Figure 4d). Finally, the average Isoprene-
638 OA mass concentration was 0.9 ± 0.5 $\mu\text{g m}^{-3}$ and composed of 59% SVOCs and 41%
639 LVOCs. Its estimated average volatility was $C^* = 1.05 \pm 0.30$ $\mu\text{g m}^{-3}$ and its vaporization
640 enthalpy was 63 ± 15 kJ mol⁻¹. Even though Isoprene-OA had a very distinct thermogram
641 compared to that of MO-OOA, their estimated volatility distribution at 25°C was very
642 atkesimilar. However, at higher temperatures (e.g., at 100°C) the remaining MO-OOA
643 after the TD was composed almost entirely of $C^* = 0.1$ $\mu\text{g m}^{-3}$, while thefor remaining
644 Isoprene-OA included material of higher volatility. the $C^* = 0.1$ $\mu\text{g m}^{-3}$ species was 0.7.
645 Finally, Isoprene-OA had much lower vaporization enthalpy than MO-OOA.

646 These results suggest that all factors contained components with a wide range of
647 volatilities and vaporization enthalpy. Based on their average volatility, BBOA was the
648 least volatile, followed by MO-OOA, Isoprene-OA and finally LO-OOA-OOA was the
649 more volatile OA component. The availability of measurements at only only three
650 temperatures above ambient, however, introduces uncertainty in the above results. A
651 detailed sensitivity analysis is presented in Section 5.

652 TFinally, the correlation between the MFR of each factor at each temperature
653 with the RH, temperature, O₃, NO, NO₂, acidity and OA loading was also investigated.
654 There was a tendency of the MFR of all factors at higher temperatures to increase as the
655 ozone concentration increased. For example, the R^2 between O₃ and the MFR of MO-
656 OOA at 80°C was 0.25, $R^2 = 0.36$ for the MFR of LO-OOA at 100°C, $R^2 = 0.26$ for the
657 MFR of Isoprene OA at 100°C and $R^2 = 0.22$ for the MFR of BBOA at 100°C. This
658 suggests that when the photochemistry is more intense the OA evaporates less in the TD.
659 The R^2 between the acidity and the MFR of LO-OOA at 100°C was 0.26, suggesting that
660 acidity may be also affecting the MFR. The MFR of BBOA at 100°C on the other hand
661 was anti-correlated towith the NO and NO₂ concentrations (R^2 of 0.23 and 0.37
662 correspondingly). This indicates that at lower NO_x levels (away from the source) BBOA
663 evaporated less, suggesting that this factor may contain both fresh and aged BBOA or
664 fresh BBOA aerosols mixed with aged background. This is also supported by the
665 relatively high O:C ratio of this factor (0.58). All the other R^2 values examined were
666 lower than 0.2. There was no distinct diurnal profile for the MO-OOA, BBOA and

Formatted: Font: Italic

Formatted: Font: Italic

Formatted: Font: Italic

Formatted: Font: Italic

Formatted: Font: Italic

Formatted: Font: Italic

Formatted: Font: Italic

667 Isoprene-OA MFR. For LO-OOA MFR at 80°C and 100°C there was a slight increase
668 (with a lot of considerable noise though) between 11:00-16:00. As a result, we do not
669 have much evidence to support a significant diurnal variation of the MFR of the various
670 factors ~~lacks support~~ was not observed.

671

672 5. Sensitivity analysis

673 5.1 Effective enthalpy of vaporization (ΔH_{vap})

674 We estimated the volatility distributions for three fixed vaporization enthalpies: 50, 80
675 and 100 kJ mol⁻¹ for all factors (Table S2). While the corresponding thermograms do not
676 reproduce as well the corresponding measurements, it is instructive to examine the
677 corresponding volatility distributions taking into account this time the measurement
678 uncertainties.

679 The 80 and 100 kJ mol⁻¹ values lead to thermograms for MO-OOA consistent with
680 the measurements given the uncertainty of the latter (Figure A1, Appendix). The resulting
681 MO-OOA volatility distributions (Figure A2, Appendix) are within the uncertainty range
682 of the distributions shown in Figure 3. The LVOC content of the factor varies from 35%
683 to 60% as the ΔH_{vap} varies from 80 to 100 kJ mol⁻¹. The optimum (base case) solution
684 suggested a 44% LVOC content.

685 The situation is a little more complex for LO-OOA due to the higher variability of
686 the corresponding MFR measurements. All three ΔH_{vap} values lead to solutions that are
687 consistent with the observations within experimental uncertainty. This results in a wide
688 range of volatility distributions with the LVOC content varying from 25% to 90% (Figure
689 A2). The best (base case) solution suggested 27% LVOCs, so the sensitivity analysis
690 suggests that the LO-OOA may have been significantly less volatile.

691 Only the 50 and 80 kJ mol⁻¹ values lead to acceptable thermograms for the
692 Isoprene OA (Figure A1). The LVOCs are predicted to contribute to the factor from 35 to
693 75% (Figure A2) as the assumed ΔH_{vap} varies from 50 to 80 kJ mol⁻¹. The optimum (base
694 case) solution corresponded to 41% LVOCs.

695 Finally, for the BBOA as the ΔH_{vap} varies from 50 to 80 kJ mol⁻¹ (the 100 kJ
696 mol⁻¹ value does not lead to acceptable solutions) the LVOC content increases from 65 to

Formatted: Font: Italic

Formatted: Font: Italic

Formatted: Font: Italic

Formatted: Font: Italic

Formatted: Font: Italic

697 87% (Figure A2), values that are higher than the estimated 47% LVOCs in the optimum
698 (base case) solution.

699

700 5.2 Accommodation coefficient

701 It has been assumed in the analysis so far that there were no resistances to the
702 evaporation of the OA in the TD and that the accommodation coefficient, a_m , was equal
703 to one. We performed two sensitivity tests using accommodation coefficients of one and
704 two orders of magnitude lower (0.1, 0.01). The volatility distributions, the average
705 volatility C^* and the vaporization enthalpy of each factor are given in Table S1. The
706 corresponding MFRs are illustrated in Figure A3 and the volatility distributions in Figure
707 A4.

708 A value of a_m equal to 0.01 is inconsistent with the measured thermograms of
709 MO-OOA, Isoprene-OA and total OA (Figure A3). For LO-OOA and BBOA the
710 predicted thermograms are within the experimental error of the measured values and the
711 resulting volatility distributions are quite close to those of the base case. For example, for
712 LO-OOA the LVOC content is 40% (Figure A4) compared to 27% in the optimum
713 solution. ~~This rather surprising insensitivity of the volatility distribution is that the model
714 balances the effects of the lower a_m with an increase of the predicted ΔH_{vap} .~~ This rather
715 surprising insensitivity of the volatility distribution is ~~because~~ due to the fact that the
716 model balances the effects of the lower a_m ~~an~~ by increasing the predicted ΔH_{vap} . In the
717 case of the LO-OOA the estimated enthalpy of vaporization increases to 121 kJ mol⁻¹.

718 The intermediate value of $a_m=0.1$ leads to predicted MFR values within the
719 experimental error for LO-OOA, Isoprene-OA and BBOA, but not for MO-OOA or total
720 OA (Figure A3). For the acceptable cases the average volatility of the OA components
721 decreases by a factor of 2-3 and the effective ΔH_{vap} increases by 30-40 kJ mol⁻¹. The
722 LVOC content of LO-OOA increases from 27% to 52%, while the increase of the
723 Isoprene-OA and BBOA LVOCs is small (from 41 to 47% and from 60 to 64%)
724 respectively (Figure A4).

725 For the MO-OOA and the total OA only the $a_m=1$ simulations provided
726 ~~aceepable~~ results consistent with the observations.

Formatted: Font: Italic

Formatted: Font: Italic

Formatted: Font: Not Italic

Formatted: Font: Italic

Formatted: Font: Italic

Formatted: Font: Italic

727 The above analysis suggests that the estimated volatility distributions have a
728 surprisingly low sensitivity to the assumed *accommodation* (evaporation) coefficient, but
729 the ΔH_{vap} is quite sensitive to this value. This result is quite different from other studies
730 (e.g., Lee et al., 2010; Cappa and Jimenez 2010; Riipinen et al., 2010) and is due to the
731 limited temperature range of the measurements in the present work.

Formatted: Font: Italic

732

733 **5.3 TD collection efficiency**

734 In this case we repeated the calculations assuming a lower AMS CE for the
735 aerosol that passed through the TD. Assuming a 10% lower CE in the TD, the volatility
736 distribution of MO-OOA and Isoprene-OA changed by less than 10% (Table S1).
737 However, the volatility distribution of LO-OOA and BBOA shifted towards lower values
738 with the average volatility decreasing by around a factor of 2. The reasons for this
739 behavior could be the high LO-OOA MFR uncertainty and the low mass concentration of
740 the BBOA. The corresponding thermograms and volatility distribution are shown in
741 Figures S4 and S5.

742

743 **6. Comparisons with other studies**

744 *MO-OOA and LO-OOA*: The volatility distributions of the MO-OOA and LO-OOA
745 were similar to those of the aged aerosol in Finokalia (FAME-08) (Lee et al., 2010) in
746 which the SVOCs accounted for 60% and LVOCs for 40% of the OA using an $a_m=0.05$
747 and $\Delta H_{vap}=80 \text{ kJ mol}^{-1}$ (Figure S67). The SOAS LO-OOA appears to be a little more
748 volatile than the summertime SV-OOA in Paris (Paciga et al., 2016) and Mexico City
749 (Cappa et al., 2010), while the MO-OOA is a lot more volatile than the LV-OOA in these
750 locations. These summertime OOA components in SOAS were more volatile compared
751 to the wintertime OOA in Paris and Athens (Louvaris et al., 2017), which had a lower
752 SVOC content (45% for Paris and 31% in Athens).

Formatted: Font: Italic

753

754 *BBOA*: Figure S6b illustrates the volatility comparisons between the BBOA factor and
755 the BBOA factors from Mexico City, Paris (winter) and Athens (winter). The estimated
756 SVOC content of all four BBOA factors was surprisingly similar around 50% with the
757 Mexico City BBOA having the higher fraction (70%). The differences in LVOCs and

758 ELVOCs are at least partially due to the temperature ranges used in the corresponding
759 measurements. The corresponding O:C ratios of the factors were quite different, 0.58 for
760 SOAS, 0.4 for Mexico City, 0.29 for Paris, and 0.23 for Athens (all estimated using the
761 Canagaratha et al. (2015) approach). Part of the reason of the discrepancy may be hidden
762 in the least volatile components of BBOA that were not examined in the present study.

763

764 ***Isoprene-OA***: Lopez-Hilfiker et al. (2016) suggested that the IEPOX SOA had much
765 lower saturation concentration, $C^*=10^{-4}$ $\mu\text{g m}^{-3}$, compared to the volatility of the
766 Isoprene-OA estimated here. However, Lopez-Hilfiker et al. (2016) results are strictly for
767 the IEPOX SOA which is a subset of the Isoprene-OA investigated here. So, a
768 quantitative comparison of the corresponding volatilities is not possible. Also, the
769 analysis of Lopez-Hilfiker et al. (2016) does not account for the effect of the vaporization
770 enthalpy. There is of course also a potentially important experimental difference in this
771 case, as in our work the OA just evaporates in the TD, while the Lopez-Hilfiker et al.
772 (2016) experimental approach involves collection of the OA on a filter and then heating
773 and desorption. Potential reasons for the discrepancy may include the fact that their
774 conclusion was based on major components of IEPOX SOA and not all the products, the
775 fact that Isoprene OA factor may not be entirely composed of IEPOX, potential
776 interactions of these components with the substrate used in FIGAERO-CIMS, the role of
777 the vaporization enthalpy in the thermal behavior of these compounds, etc. As a
778 consistency test, we used the volatility distribution of Lopez-Hilfiker et al. (2016) as
779 input to the code of Riipinen et al. (2010) varying the enthalpy of vaporization. The best
780 result was obtained for an abnormally high value of $\Delta H_{\text{vap}}=208$ kJ mol^{-1} and even then the
781 model underestimates the observed evaporation of Isoprene-OA (Figure S7). Using more
782 reasonable values of ΔH_{vap} for such compounds the discrepancies between our
783 measurements and the predictions are even larger, suggesting that the Lopez-Hilfiker et al.
784 (2016) volatility estimates are not consistent with our results and appear not to represent
785 the full volatility range of Isoprene-OA.

786 A similar discrepancy exists with the low estimated volatility for the IEPOX SOA
787 by Hu et al. (2016) which is even lower than that of Lopez-Hilfiker et al. (2016) (Figure
788 S6c). Even though Hu et al. (2016) used the same AMS-thermodenuder technique, their

Formatted: Font: Italic

Formatted: Font: Italic

789 [approach for the measurement interpretation was very different. Hu et al. \(2016\) used the](#)
790 [empirical method of Faulhaber et al. \(2009\) and not an aerosol dynamic model for the](#)
791 [estimation of the volatility distributions from their MFR measurements. Their method](#)
792 [was based on a relationship between TD temperature and organic species saturation](#)
793 [concentration at 298 K \(\$C^*\$ \) that has been obtained using 5 compounds \(acids\) with](#)
794 [known saturation concentration. This approach is applicable to organic compounds with](#)
795 [similar properties \(e.g., enthalpy of vaporization\) to the 5 known compounds, but it may](#)
796 [encounter significant difficulties for OA that is quite different from the model compounds.](#)
797 [A related weakness of that approach is that it does not account for the enthalpy of](#)
798 [vaporization as the model used in this work does. One reason for the discrepancy is that](#)
799 [their estimate was based on the empirical method of Faulhaber et al. \(2009\) which has](#)
800 [been calibrated using the TD behavior of 5 known compounds and neglecting potential](#)
801 [differences in \$\Delta H_{\text{vap}}\$.](#)

802 These discrepancies clearly show that there is need for additional investigation of
803 the volatility of the various components of the isoprene SOA in the atmosphere.

804
805 **Total OA:** Figure S6d compares the total OA volatility estimated in this study to those of
806 Lopez-Hilfiker et al. (2016), Hu et al. (2016), and Saha et al. (2017) for the same location
807 (Centreville) and period. To facilitate the comparison, given that different temperature
808 ranges were used in the above studies, the $C^*=0.1 \mu\text{g m}^{-3}$ bin is used to represent
809 compounds of even lower volatility than this value. Our results are quite consistent with
810 those of Saha et al. (2017) especially considering the differences in both the TD design
811 and modeling of the results. [Saha et al. \(2017\) obtained the total OA thermogram using a](#)
812 [thermodenuder system and then estimated the corresponding volatility distribution using](#)
813 [an aerosol dynamics model and the volatility basis set \(Donahue et al., 2006; Lee et al.,](#)
814 [2011; Saha et al., 2015; Saha and Grieshop, 2016\). Their experimental and data analysis](#)
815 [approach is a lot closer to ours compared to Hu et al. \(2016\) and Lopez-Hilfiker et al.](#)
816 [\(2016\) and their results for the total OA are quite consistent with ours. Their model takes](#)
817 [into account the vaporization enthalpy as well and this is probably the key difference](#)
818 [among the various approaches. On the other hand, the Hu et al. \(2016\) and Lopez-Hilfiker](#)

819 [et al. \(2016\) results suggest an OA with much lower volatility that is inconsistent with](#)
820 [our TD measurements.](#)

821

822 **7. Link to the 2D-VBS framework**

823 Figure [54](#) shows the location of our factors in the 2D-VBS framework of
824 Donahue et al. (2012). The PMF sources locations in the 2D-VBS were estimated using
825 the elemental ratios derived by the method of Aiken et al. (2008) for consistency with the
826 original figure. The O:C of the MO-OOA, LO-OOA, Isoprene-OA and BBOA factors
827 was 0.8, 0.46, 0.44 and 0.46 correspondingly. The MO-OOA factor is in the proposed
828 LV-OOA area but it includes a SVOC component that does not exist in the original 2D-
829 VBS. The LO-OOA factor is quite consistent with the proposed SV-OOA area. The
830 Isoprene-OA is also located in the SV-OOA area based on our results. Finally, the BBOA
831 factor has the expected volatility range, but is in the upper border of the 2D-VBS BBOA
832 area due to its high oxidation state observed during SOAS.

833

834 **8. Linking the hygroscopicity of OA components to their O:C ratio and volatility**

835 Cerrully et al. (2015) estimated the hygroscopicity κ parameter for each factor for
836 the SOAS campaign for supersaturation $s=0.4\%$ using PMF analysis on the PILS aerosol.
837 The resulting values were: $\kappa_{\text{MO-OOA}}=0.16\pm 0.02$, $\kappa_{\text{LO-OOA}}=0.08\pm 0.02$ and $\kappa_{\text{Isoprene-OA}}=$
838 0.20 ± 0.02 . During the periods of the PILS measurements the BBOA contribution was
839 very low and PMF could not resolve this factor. The Isoprene-OA factor had a higher κ
840 than MO-OOA, but its O:C ratio was lower (0.62) than MO-OOA (1.02). This contradicts
841 Jimenez et al. (2009) which proposed that the hygroscopicity increases linearly as the
842 O:C ratio increases and the recent study of Thalman et al. (2017) which suggested that for
843 OOA factors the relationship between the hygroscopicity and the O:C is linear. [A](#)
844 [possible explanation for this contradiction could be that the O:C-hygroscopicity](#)
845 [relationship may not be monotonic, but there may be systems for ~~which~~ ~~the~~ which the](#)
846 [relationship may be highly nonlinear. For example, Cain and Pandis \(2017\) showed that](#)
847 [the hygroscopicity could exhibit a maximum at intermediate volatilities.](#)

848 A recent study by Nakao (2017) proposed a theoretical description for the linkage
849 between the O:C ratio, volatility and hygroscopicity. Figure S8 illustrates the

850 experimental saturation concentrations and κ parameters for known compounds found in
851 the literature (Table S3 and S4) together with the Nakao (2017) estimations. The isolines
852 in this figure represent the intrinsic κ which corresponds to the upper limit of κ assuming
853 that the organic species are entirely soluble. The location of the selected known
854 compounds was generally in agreement with the suggested by Nakao (2017) intrinsic κ
855 isolines for κ higher than 0.1. For κ lower than 0.1 the experimental values were
856 underestimated compared to the theoretical κ . This discrepancy could be due to the fact
857 that the compounds in the area with κ above 0.1 are more water soluble than those in the
858 area with κ below 0.1. For example, the solubility of malonic acid is 1161 g L^{-1} (Saxena
859 and Hildemann 1996), while the water solubility of suberic acid is 2.46 g L^{-1} (Bretti et al.,
860 2006).

861 Xu et al. (2017) calculated the water solubility of the MO-OOA, LO-OOA and
862 Isoprene-OA in Centreville during the SOAS campaign and found it 100%, 47% and 83%
863 correspondingly. Thus, the intrinsic κ of MO-OOA, LO-OOA and Isoprene-OA is
864 correspondingly 0.16 ± 0.02 , 0.17 ± 0.04 and 0.24 ± 0.03 . Figure 65 shows the intrinsic κ
865 values of our factors in the 2D-VBS and the Nakao (2017) frameworks. The MO-OOA
866 and LO-OOA values are close to the Nakao (2017) proposed intrinsic κ isolines.
867 However, the Isoprene-OA experimental intrinsic κ (0.24) is higher than the theoretical
868 (0.13). One reason for this disagreement could be the O:C estimate by the AMS.
869 Canagaratna et al. (2015) measured the O:C ratio of a racemic mixture of δ -Isoprene
870 epoxydiols ($\text{C}_5\text{H}_{10}\text{O}_3$) and found it around 0.4, which is 1.5 times lower than the
871 theoretical (0.6). If the Isoprene-OA factor behaves similarly to the racemic mixture, its
872 O:C may in fact be as high as 0.9, corresponding to a higher theoretical (Nakao 2017)
873 intrinsic $\kappa=0.19$, which is closer to the experimental value (0.24). Although our results
874 cannot be fully explained by the theoretical framework of (Nakao 2017), they denote that
875 the relationship between hygroscopicity, volatility and O:C ratio is rather complicated.
876 The model of Nakao (2017) is based on numerous assumptions that may not always be
877 valid and which could introduce errors in the κ isolines estimation. Recently, Rastak et al.
878 (2017) concluded that the hygroscopicity should be described using more than a single
879 parameter. In addition, [Cain Kerrigan](#) and Pandis (2017) suggested that the
880 hygroscopicity could exhibit a maximum at intermediate volatilities.

881
882
883
884
885
886
887
888
889
890
891
892
893
894
895
896
897
898
899
900
901
902
903
904
905
906
907
908
909
910
911

9. Conclusions

The volatility distribution of the OA factors found during the SOAS campaign was estimated using measurements by a thermodenuder coupled with a HR-AMS. Using both the ambient and the thermodenuder data the same four sources were identified compared to the ambient only PMF analysis. The four sources were attributed to MO-OOA, LO-OOA, Isoprene-OA and BBOA. The contribution, the times series and the mass spectra of each factor were similar to the case of the ambient-only PMF. Using the MFRs and the thermodenuder model of Riipinen et al. (2010) the volatility distribution and the vaporization enthalpy of each factor was estimated assuming an accommodation coefficient of unity.

MO-OOA was significantly more oxygenated than LO-OOA, but in contrast with previous studies, its MFR was much lower. According to the model, the MO-OOA was less volatile than the LO-OOA and the implausible behavior of the measured MFR was due to their different effective enthalpies of evaporation: 89 ± 10 kJ mol⁻¹ for the MO-OOA and 58 ± 13 kJ mol⁻¹ for the LO-OOA. Isoprene-OA had a similar volatility distribution with MO-OOA, but its vaporization enthalpy was lower at 63 ± 15 kJ mol⁻¹. BBOA had the lowest O:C ratio but it was the least volatile OA component with a vaporization enthalpy of 55 ± 11 kJ mol⁻¹. All factors, included components with a wide range of volatilities, both semi-volatile and low volatility. The use of a relatively modest highest temperature (100°C) did not allow the characterization of the least volatile components of the various factors. The above results suggest that variations in the enthalpy of vaporization can introduce significant variability in the links between the measured MFR and the estimated volatility. [We strongly recommend the use of higher temperatures in additional steps in future studies.](#)

The contradicting result of the higher MFR of the MO-OOA compared to that of LO-OOA denotes that depending on the study the behavior of the OOA factors can be quite variable. It shows that OOA factors are composed of organic compounds with a wide range of volatility distributions, which may overlap a lot with each other. One possible reason could be the existence of small highly oxygenated molecules. [However, the HR-ToF-AMS cannot provide detailed information about the identity of the](#)

912 [compounds in each volatility bin and so, the use of other chemical analysis techniques is](#)
913 [required.](#) The direct comparison of the MFR of OOA factors from different or even from
914 the same study is risky since MFR depends on the TD operation and characteristics, the
915 aerosol size distribution, the volatility, etc. [The effective enthalpy of vaporization is a](#)
916 [parameter that it has to be taken under consideration when we estimate volatility](#)
917 [distributions. It may explain why the contradiction the relationship between between-MO-](#)
918 [OOA and LO-OOA MFR and volatility is complex and the apparent paradox similarity](#)
919 [between the MO-OOA and Isoprene-OA volatility distributions. However, in the second](#)
920 [case the uncertainties of the Isoprene-OA volatility distribution for all bins were](#)
921 [significant. There are solutions for which the MO-OOA is a lot less volatile than the](#)
922 [Isoprene-OA. So the measurements in this case are not sufficient to compare the](#)
923 [volatilities of the two factors.](#)

924 ~~[This is the reason that we did our best in the study to avoid strong conclusions](#)~~
925 ~~[about comparisons of the volatilities of the various factors.](#)~~

926 The counterintuitive finding of Cerully et al. (2015), that Isoprene-OA was more
927 hygroscopic than MO-OOA even though it had a lower O:C ratio, but similar volatility
928 distribution, are close but not fully explained by the framework proposed by Nakao
929 (2017). [The proposed relationship of Jimenez et al. \(2009\) does may not apply to all](#)
930 [environments and especially when multiple aerosol sources and types are present. This](#)
931 [suggests that the relationship between the hygroscopicity and the volatility may also be](#)
932 [highly nonlinear.](#) Future studies are necessary for a comprehensive understanding of the
933 relationship between the hygroscopicity, volatility and O:C ratio.

934

935 **Acknowledgments**

936 This work was funded by the National Oceanic and Atmospheric Administration CPO
937 Award NA10OAR4310102 and the US Environmental Protection Agency (EPA-STAR)
938 through grants RD-835410 and RD-835405. This research was also supported by the
939 European Research Council Project PyroTRACH (Pyrogenic TRansformations Affecting
940 Climate and Health) Grant Agreement 726165. AN, LX, HG, RW and NLN acknowledge
941 support from an NSF grant (1242258). LX and NLN acknowledge support from EPA
942 STAR grant RD-83540301. [The authors acknowledge the Atmospheric Research and](#)

943 [Analysis Institute \(ARA\) for providing meteorological and gas phase species data.](#) The
944 contents of this publication are solely the responsibility of the authors and do not
945 necessarily represent the official views of the US EPA. Further, the US EPA does not
946 endorse the purchase of any commercial products or services mentioned in the
947 publication.

948
949
950
951
952
953
954
955
956
957

958 **References**

- 959 Aiken, A. C. et al.: O/C and OM/OC ratios of primary, secondary, and ambient organic
960 aerosols with High Resolution Time-of-Flight Aerosol Mass Spectrometry,
961 Environ. Sci. Technol., 42, 4478–4485, 2008.
- 962 Aiken, A. C. et al.: Mexico City aerosol analysis during MILAGRO using high resolution
963 aerosol mass spectrometry at the urban supersite (T0) – Part 1: Fine particle
964 composition and organic source apportionment, Atmos. Chem. Phys., 9, 6633–
965 6653, 2009.
- 966 An, W. J., Pathak, R. K., Lee, B. H., and Pandis, S. N.: Aerosol volatility measurement
967 using an improved thermodenuder: Application to secondary organic aerosol, J.
968 Aerosol Sci., 38, 305–314, 2007.
- 969 Asa-Awuku, A., Engelhart, G. J., Lee, B. H., Pandis, S. N., and Nenes, A.: Relating CCN
970 activity, volatility, and droplet growth kinetics of β -caryophyllene secondary
971 organic aerosol, Atmos. Chem. Phys., 9, 795–812, 2009.
- 972 Bretti, C., Crea, F., Foti, C., and Sammartano, S.: Solubility and activity coefficients of
973 acidic and basic nonelectrolytes in aqueous salt solutions. 2. Solubility and

974 activity coefficients of suberic, azelaic, and sebacic acids in NaCl(aq),
975 (CH₃)₄NCl(aq), and (C₂H₅)₄NI(aq) at different ionic strengths and at t = 25 °C, J.
976 Chem. Eng. Data., 51: 1660–1667, 2006.

977 Budisulistiorini, S. H., Nenes, A., Carlton, A. G., Surratt, J. D., McNeill, V. F., Pye, H. O.
978 T.: Simulating aqueous-phase Isoprene-Epoxydiol (IEPOX) secondary organic
979 aerosol production during the 2013 Southern Oxidant and Aerosol Study (SOAS),
980 Environ. Sci. Technol., 51, 5026-5034, 2017.

981 Burtscher, H., Baltensperger, U., Bukowiecki, N., Cohn, P., Hüglin, C., Mohr, M., Matter,
982 U., Nyeki S., Schmatloch V., Streit, N., and Weingartner, E.: Separation of
983 volatile and non-volatile aerosol fractions by thermodesorption: Instrumental
984 development and applications, J. Aerosol Sci., 32, 427–442, 2001.

985 Canagaratna, M. R., Jimenez, J. L., Kroll, J. H., Chen, Q., Kessler, S. H., Massoli, P.,
986 Hildebrandt Ruiz, L., Fortner, E., Williams, L. R., Wilson, K. R., Surratt, J. D.,
987 Donahue, N. M., Jayne, J. T., and Worsnop, D. R.: Elemental ratio measurements
988 of organic compounds using aerosol mass spectrometry: characterization,
989 improved calibration, and implications, Atmos. Chem. Phys., 15, 253-272, 2015.

990 Cappa, C. D. and Jimenez, J. L.: Quantitative estimates of the volatility of ambient
991 organic aerosol, Atmos. Chem. Phys., 10, 5409–5424, 2010.

992 Carlton, A.G. et al.: The Southeast Atmosphere Studies (SAS): Coordinated investigation
993 and discovery to answer critical questions about fundamental atmospheric
994 processes, Bul.Am.Met.Soc., in review, 2017.

995 Cain, K. P. and Pandis, S. N.: A technique for the measurement of organic aerosol
996 hygroscopicity, oxidation level, and volatility distributions, Atmos. Meas. Tech.
997 Discuss., amt-2017-213, in review, 2017.

998 Cerully, K. M., Hite, J., McLaughlin, M., and Nenes, A.: Towards the determination of
999 joint volatility-hygroscopicity distributions: instrument development and response
1000 characterization for single-component aerosol, Aerosol. Sci. Tech., 48, 296–312,
1001 2014.

1002 Cerully, K. M., Bougiatioti, A., Hite Jr., J. R., Guo, H., Xu, L., Ng, N. L., Weber, R., and
1003 Nenes, A.: On the link between hygroscopicity, volatility, and oxidation state of

1004 ambient and water-soluble aerosols in the southeastern United States, Atmos.
1005 Chem. Phys., 15, 8679-8694, 2015.

1006 Chang, R. Y.-W., Slowik, J. G., Shantz, N. C., Vlasenko, A., Liggio, J., Sjostedt, S. J.,
1007 Leaitch, W. R., and Abbatt, J. P. D.: The hygroscopicity parameter (κ) of ambient
1008 organic aerosol at a field site subject to biogenic and anthropogenic influences:
1009 relationship to degree of aerosol oxidation, Atmos. Chem. Phys., 10, 5047–5064,
1010 2010.

1011 Chen, N. H., and Othmer, D. F.: New generalized equation for gas diffusion coefficient, J.
1012 Chem. Eng. Data, 7, 37-41, 1962.

1013 Cohen A. J. et al.: Estimates and 25-year trends of the global burden of disease
1014 attributable to ambient air pollution: an analysis of data from the Global Burden
1015 of Diseases Study 2015, The Lancet, 389, 10082, 1907–1918, 2017.

1016 Crippa, M., et al.: Wintertime aerosol chemical composition and source apportionment of
1017 the organic fraction in the metropolitan area of Paris, Atmos. Chem. Phys., 13,
1018 961–981, 2013.

1019 DeCarlo, P.F., Kimmel, J. R., Trimborn, A., Northway, M. J., Jayne, J. T., Aiken, A. C.,
1020 Gonin, M., Fuhrer, K., Horvath, T., Docherty, K., Worsnop, D. R., and Jimenez, J.
1021 L.: Field-Deployable, High-Resolution, Time-of-Flight Aerosol Mass
1022 Spectrometer, Analytical Chemistry, 78: 8281-8289, 2006.

1023 [Donahue, N. M., Robinson, A. L., Stanier, C. O., and Pandis, S. N.: Coupled Partitioning,
1024 Dilution, and Chemical Aging of Semivolatile Organics, Environ. Sci. Technol.,
1025 40, 2635–2643, 2006.](#)

1026 Donahue, N. M., Kroll, J. H., Pandis, S. N., and Robinson, A. L.: A two-dimensional
1027 volatility basis set – Part 2: Diagnostics of organic-aerosol evolution, Atmos.
1028 Chem. Phys., 12, 615–634, 2012.

1029 Faulhaber, A. E., Thomas, B. M., Jimenez, J. L., Jayne, J. T., Worsnop, D. R., and
1030 Ziemann, P. J.: Characterization of a thermodenuder-particle beam mass
1031 spectrometer system for the study of organic aerosol volatility and composition,
1032 Atmos. Meas. Tech., 2, 15-31, 2009.

1033 Florou, K., Papanastasiou, D. K., Pikridas, M., Kaltsonoudis, C., Louvaris, E., Gkatzelis,
1034 E., Patoulias, D., Mihalopoulos, N., and Pandis, S. N.: The contribution of wood

Formatted: English (United States)

Formatted: English (United States)

Formatted: English (United States)

1035 burning and other pollution sources to wintertime organic aerosol levels in two
1036 Greek cities, *Atmos. Chem. Phys.*, 17, 3145-3163, 2017.

1037 Frosch, M., Bilde, M., Nenes, A., Praplan, A. P., Jurányi, Z., Dommen, J., Gysel, M.,
1038 Weingartner, E., and Baltensperger, U.: CCN activity and volatility of β -
1039 caryophyllene secondary organic aerosol, *Atmos. Chem. Phys.*, 13, 2283–2297,
1040 2013.

1041 Fuchs, N.A., and Sutugin, A.G.: *Highly Dispersed Aerosols*. Ann Arbor Science
1042 Publishers, Ann Arbor, London, 1970.

1043 Guo, H., Xu, L., Bougiatioti, A., Cerully, K. M., Capps, S. L., Hite Jr., J. R., Carlton, A.
1044 G., Lee, S.-H., Bergin, M. H., Ng, N. L., Nenes, A., and Weber, R. J.: Fine-
1045 particle water and pH in the southeastern United States, *Atmos. Chem. Phys.*, 15,
1046 5211-5228, 2015.

1047 Hallquist, M. J. C. et al.: The formation, properties and impact of secondary organic
1048 aerosol: current and emerging issues, *Atmos. Chem. Phys.*, 9, 5155-5236, 2009.

1049 Hu, W. et al.: Characterization of a real-time tracer for isoprene epoxydiols-derived
1050 secondary organic aerosol (IEPOX-SOA) from aerosol mass spectrometer
1051 measurements, *Atmos. Chem. Phys.*, 15, 11807-11833, 2015.

1052 Hu, W. et al.: Volatility and lifetime against OH heterogeneous reaction of ambient
1053 isoprene-epoxydiols-derived secondary organic aerosol (IEPOX-SOA), *Atmos.*
1054 *Chem. Phys.*, 16, 11563-11580, 2016.

1055 Huffman, J. A., Docherty, K. S., Aiken, A. C., Cubison, M. J., Ulbrich, I. M., DeCarlo, P.
1056 F., Sueper, D., Jayne, J. T., Worsnop, D. R., Ziemann, P. J., and Jimenez, J. L.:
1057 Chemically-resolved aerosol volatility measurements from two megacity field
1058 studies, *Atmos. Chem. Phys.*, 9, 7161–7182, 2009.

1059 Jimenez, J. L. et al.: Evolution of organic aerosols in the atmosphere, *Science*, 326,
1060 1525–1529, 2009.

1061 IARC (International Agency for Research on Cancer). In press. *Outdoor Air Pollution*.
1062 IARC Monogr. Eval. Carcinog. Risks Hum 109.

1063 IPCC, Intergovernmental Panel on Climate Change, *Climate change 2013: The Physical*
1064 *Science Basis*. Cambridge University Press, Cambridge, 2013.

1065 Kanakidou, M. et al.: Organic aerosol and global climate modelling: a review, *Atmos.*
1066 *Chem. Phys.*, 5, 1053-1123, 2005.

1067 Karnezi, E., Riipinen, I., and Pandis, S. N.: Measuring the atmospheric organic aerosol
1068 volatility distribution: a theoretical analysis, *Atmos. Meas. Tech.*, 7, 2953–2965,
1069 2014.

1070 Kostenidou, E., Florou, K., Kaltsonoudis, C., Tsiflikiotou, M., Vratolis, S., Eleftheriadis,
1071 K., and Pandis, S. N.: Sources and chemical characterization of organic aerosol
1072 during the summer in the eastern Mediterranean, *Atmos. Chem. Phys.*, 15, 11355-
1073 11371, 2015.

1074 Kostenidou, E., Karnezi, E., Kolodziejczyk, A., Szmigielski, R., and Pandis, S. N.:
1075 Physical and chemical properties of 3-methyl-1,2,3-butanetricarboxylic acid
1076 (MBTCA) aerosol, *Environ. Sci.-Technol.*, [52 \(3\), 1150-1155, 2018.](#)
1077 [submitted, 2017.](#)

1078 Kuwata, M., Kondo, Y., Mochida, M., Takegawa, N., and Kawamura, K.: Dependence of
1079 CCN activity of less volatile particles on the amount of coating observed in Tokyo,
1080 *J. Geophys. Res.*, 112, D11207, doi:10.1029/2006JD007758, 2007.

1081 Lanz, V. A., Alfarra, M. R., Baltensperger, U., Buchmann, B., Hueglin, C., and Prévôt, A.
1082 S. H.: Source apportionment of submicron organic aerosols at an urban site by
1083 factor analytical modeling of aerosol mass spectra, *Atmos. Chem. Phys.*, 7, 1503–
1084 1522, 2007.

1085 Lanz, V. A., Alfarra, M. R., Baltensperger, U., Buchmann, B., Hueglin, C., Szidat, S.,
1086 Wehrli, M. N., Wacker, L., Weimer, S., Caseiro, A., Puxbaum, J., and Prévôt, A.
1087 S. H.: Source attribution of submicron organic aerosols during wintertime
1088 inversions by advanced factor analysis of aerosol mass spectra, *Environ. Sci.*
1089 *Technol.*, 42, 214-220, 2008.

1090 Latham, T. L., Beyersdorf, A. J., Thornhill, K. L., Winstead, E. L., Cubison, M. J.,
1091 Hecobian, A., Jimenez, J. L., Weber, R. J., Anderson, B. E., and Nenes, A.:
1092 Analysis of CCN activity of Arctic aerosol and Canadian biomass burning during
1093 summer 2008, *Atmos. Chem. Phys.*, 13, 2735–2756, 2013.

1094 Lee, B. H., Kostenidou, E., Hildebrandt, L., Riipinen, I., Engelhart, G. J., Mohr, C.,
1095 DeCarlo, P. F., Mihalopoulos, N., Prevot, A. S. H., Baltensperger, U., and Pandis,

1096 S. N.: Measurement of the ambient organic aerosol volatility distribution:
1097 application during the Finokalia Aerosol Measurement Experiment (FAME-
1098 2008). *Atmos. Chem. Phys.*, 10, 12149-12160, 2010.

1099 Lee, B. H., Pierce, J. R., Engelhart, G. J., and Pandis, S. N.: Volatility of secondary
1100 organic aerosol from the ozonolysis of monoterpenes. *Atmos. Environ.*, 45, 2443-
1101 2452, 2011.

1102 Liao, H., Henze, D. K., Seinfeld, J. H., Wu, S., and Mickley, L. J.: Biogenic secondary
1103 organic aerosol over the United States: Comparison of climatological simulations
1104 with observations, *J. Geophys. Res.*, 112, D06201, doi:10.1029/2006JD007813,
1105 2007.

1106 Lopez-Hilfiker, F. D., Mohr, C., D'Ambro, E. L., Lutz, A., Riedel, T. P., Gaston, C. J.,
1107 Iyer, S., Zhang, X., Gold, A., Surratt, J. D., Lee, B. H., Kurten, T., Hu, W. W.,
1108 Jimenez, J., Hallquist, M., and Thornton, J. A.: Molecular composition and
1109 volatility of organic aerosol in the Southeastern U.S.: Implications for IEPOX
1110 derived SOA. *Environ. Sci. Technol.*, 50, (5), 2200-2209, 2016.

1111 Louvaris, E., Florou, K., Karnezi, E., Papanastasiou, D. K., Gkatzelis, G. I., and Pandis, S.
1112 N.: Volatility of source apportioned wintertime organic aerosol in the city of
1113 Athens, *Atmos. Environ.*, 158, 138-147, 2017.

1114 Meyer, N. K., Duplissy, J., Gysel, M., Metzger, A., Dommen, J., Weingartner, E., Alfarra,
1115 M. R., Prevot, A. S. H., Fletcher, C., Good, N., McFiggans, G., Jonsson, Å. M.,
1116 Hallquist, M., Baltensperger, U., and Ristovski, Z. D.: Analysis of the
1117 hygroscopic and volatile properties of ammonium sulphate seeded and unseeded
1118 SOA particles, *Atmos. Chem. Phys.*, 9, 721–732, 2009.

1119 Middlebrook, A. M., Bahreini, R., Jimenez, J.L., and Canagaratna, M. R.: Evaluation of
1120 composition - dependent collection efficiencies for the Aerodyne Aerosol Mass
1121 Spectrometer using field data, *Aerosol Sci. Tech.*, 46, 258 - 271, 2012.

1122 Moore, R. H. and Nenes, A.: Scanning flow CCN analysis – a method for fast
1123 measurements of CCN spectra, *Aerosol Sci. Tech.*, 43, 1192–1207, 2009.

1124 Nakao, S.: Why would apparent κ linearly change with O/C? Assessing the Role of
1125 Volatility, Solubility, and Surface Activity of Organic Aerosols, *Aerosol Sci.*
1126 *Tech.*, under revision, 2017.

1127 National Academies of Sciences, Engineering, and Medicine: The Future of Atmospheric
1128 Chemistry Research: Remembering Yesterday, Understanding Today,
1129 Anticipating Tomorrow Washington, DC, The National Academies Press. doi:
1130 10.17226/235730, 2016.

1131 Ng, N. L. et al.: Organic aerosol components observed in Northern Hemispheric datasets
1132 from Aerosol Mass Spectrometry, *Atmos. Chem. Phys.*, 10, 4625–4641, 2010.

1133 Ortiz-Montalvo, D. L., Lim, Y. B., Perri, M. P., Seitzinger, S. P., and Turpin, B. J.:
1134 Volatility and yield of glycolaldehyde SOA formed through aqueous
1135 photochemistry and droplet evaporation, *Aerosol Sci. Tech.*, 46, 1002–1014, 2012.

1136 Paatero, P. and Tapper, U.: Positive matrix factorization – a nonnegative factor model
1137 with optimal utilization of error-estimates of data values, *Environmetrics*, 5, 111–
1138 126, 1994.

1139 Paciga, A., Karnezi, E., Kostenidou, E., Hildebrandt, L., Psichoudaki, M., Engelhart, G.
1140 J., Lee, B.-H., Crippa, M., Prévôt, A. S. H., Baltensperger, U., and Pandis, S. N.:
1141 Volatility of organic aerosol and its components in the megacity of Paris, *Atmos.*
1142 *Chem. Phys.*, 16, 2013–2023, 2016.

1143 Peng, C., Chan, M. N., and Chan, C. K.: The hygroscopic properties of dicarboxylic and
1144 multifunctional acids: measurements and UNIFAC predictions, *Environ. Sci.*
1145 *Technol.*, 35, 4495–4501, 2001.

1146 Pope, C. A., Burnett, R. T., Thun, M. J., Calle, E. E., Krewski, D., Ito, K., Thurston, G.
1147 D.: Lung cancer, cardiopulmonary mortality, and long-term exposure to fine
1148 particulate air pollution, *JAMA*, 287, 1132–41, 2002.

1149 Rastak, N., A. et al.: Microphysical explanation of the RH-dependent water-affinity of
1150 biogenic organic aerosol and its importance for climate, *Geoph. Res. Let.*, 44,
1151 doi:10.1002/2017GL073056, 2017.

1152 Riipinen, I., Pierce, J. R., Donahue, N. M., and Pandis, S. N.: Equilibration time scales of
1153 organic aerosol inside thermodenuders: Evaporation kinetics versus
1154 thermodynamics, *Atmos. Environ.*, 44, 597–607, 2010.

1155 Roberts, G. C., and Nenes, A.: A continuous-flow streamwise thermal-gradient CCN
1156 chamber for atmospheric measurements, *Aerosol Sci. Tech.*, 39, 206–221, 2005.

1157 [Saha, P. K., Khlystov, A., and Grieshop, A. P.: Determining Aerosol Volatility](#)
1158 [Parameters Using a “Dual Thermodenuder” System: Application to Laboratory-](#)
1159 [Generated Organic Aerosols, Aerosol Sci. Tech., 49, 620–632, 2015.](#)

Formatted: English (United States)

Formatted: English (United States)

Formatted: English (United States)

Formatted: English (United States)

1160 Saha, P. K., and Grieshop, A. P.: Exploring divergent volatility properties from yield and
1161 thermodenuder measurements of secondary organic aerosol from α -pinene
1162 ozonolysis, Environ. Sci. Technol., 50, 5740–5749, 2016.

1163 Saha, P. K., Khlystov, A., Yahya, K., Zhang, Y., Xu, L., Ng, N. L., and Grieshop, A. P.:
1164 Quantifying the volatility of organic aerosol in the southeastern US, Atmos. Chem.
1165 Phys., 17, 501-520, 2017.

1166 Saleh, R., Walkerb, J., and Khlystov, A.: Determination of saturation pressure and
1167 enthalpy of vaporization of semi-volatile aerosols: The integrated volume method,
1168 Aerosol Science, 39, 876–887, 2008.

1169 Saleh, R., Khlystov, A., and Shihadeh, A.: Effect of aerosol generation method on
1170 measured saturation pressure and enthalpy of vaporization for dicarboxylic acids
1171 aerosol, Aerosol Sci. Tech., 44, 302-307, 2010.

1172 Saleh, R., Shihadeh, A., and Khlystov, A.: On transport phenomena and equilibration
1173 time scales in thermodenuders, Atmos. Meas. Tech., 4, 571–581, 2011.

1174 Saxena, P., and Hildemann, L.: Water-soluble organics in atmospheric particles: a critical
1175 view of the literature and application of thermodynamics to identify candidate
1176 compounds. J. Atmos. Chem., 24, 57-109, 1996.

1177 Seinfeld, J. H. et al.: Improving our fundamental understanding of the role of aerosol-
1178 cloud interactions in the climate system, P. Natl. Acad. Sci., 113, 21, 5781-5790,
1179 2016.

1180 Spracklen, D. V., Jimenez, J. L., Carslaw, K. S., Worsnop, D. R., Evans, M. J., Mann, G.
1181 W., Zhang, Q., Canagaratna, M. R., Allan, J., Coe, H., McFiggans, G., Rap, A.,
1182 and Forster, P.: Aerosol mass spectrometer constraint on the global secondary
1183 organic aerosol budget, Atmos. Chem. Phys., 11, 12109-12136, 2011.

1184 Stephenson, R. M. and Malanowski, S.: Handbook of the Thermodynamics of Organic
1185 Compounds, 1987.

1186 Thalman, R. et al.: CCN activity and organic hygroscopicity of aerosols downwind of an
1187 urban region in central Amazonia: Seasonal and diel variations and impact of

1188 anthropogenic emissions, *Atmos. Chem. Phys. Discuss.*,
1189 <https://doi.org/10.5194/acp-2017-251>, in review, 2017.

1190 Tritscher, T., Dommen, J., DeCarlo, P. F., Gysel, M., Barmet, P. B., Praplan, A. P.,
1191 Weingartner, E., Prévôt, A. S. H., Riipinen, I., Donahue, N. M., and Baltensperger,
1192 U.: Volatility and hygroscopicity of aging secondary organic aerosol in a smog
1193 chamber, *Atmos. Chem. Phys.*, 11, 11477–11496, 2011.

1194 Ulbrich, I. M., Canagaratna, M. R., Zhang, Q., Worsnop, D. R., and Jimenez, J. L.:
1195 Interpretation of organic components from Positive Matrix Factorization of
1196 aerosol mass spectrometric data, *Atmos. Chem. Phys.*, 9, 2891–2918, 2009.

1197 Vesala, T., Kulmala, M., Rudolf, R., Vrtala, A., and Wagner, P. E.: Models for
1198 condensational growth and evaporation of binary aerosol particles, *J. Aerosol Sci.*
1199 28, 565-598, 1997.

1200 Weber, R. J., Orsini, D., Daun, Y., Lee, Y.-N., Klotz, P., and Brechtel, F.: A particle-into-
1201 liquid collector for rapid measurements of aerosol chemical composition, *Aerosol*
1202 *Sci. Tech.*, 35, 718–727, 2001.

1203 Xu, L., Guo, H., Boyd, C. M., Klein, M., Bougiatioti, A., Cerully, K. M., Hite, J. R.,
1204 Isaacman-VanWertz, G., Kreisberg, N. M., Knote, C., Olson, K., Koss, A.,
1205 Goldstein, A. H., Hering, S. V., de Gouw, J., Baumann, K., Lee, S.-H., Nenes, A.,
1206 Weber, R. J., and Ng, N. L.: Effects of anthropogenic emissions on aerosol
1207 formation from isoprene and monoterpenes in the Southeastern United States, *P.*
1208 *Natl. Acad. Sci.*, 112, 37–42, 2015a.

1209 Xu, L., Suresh, S., Guo, H., Weber, R. J., and Ng, N. L.: Aerosol characterization over
1210 the southeastern United States using High-Resolution Aerosol Mass
1211 Spectrometry: spatial and seasonal variation of aerosol composition and sources
1212 with a focus on organic nitrates, *Atmos. Chem. Phys.*, 15, 7307-7336, 2015b.

1213 Xu, L., et al.: Enhanced formation of isoprene-derived organic aerosol in power plant
1214 plumes during Southeast Nexus (SENEX), *J. Geoph. Res.*, 121, doi:
1215 10.1002/2016JD025156, 2016a.

1216 Xu, L., Williams, L. R., Young, D. E., Allan, J. D., Coe, H., Massoli, P., Fortner, E.,
1217 Chhabra, P., Herndon, S., Brooks, W. A., Jayne, J. T., Worsnop, D. R., Aiken, A.
1218 C., Liu, S., Gorkowski, K., Dubey, M. K., Fleming, Z. L., Visser, S., Prévôt, A. S.

1219 H., and Ng, N. L.: Wintertime aerosol chemical composition, volatility, and
1220 spatial variability in the greater London area, *Atmos. Chem. Phys.*, 16, 1139-1160,
1221 2016b.

1222 Xu, L., Guo, H., Weber, R. J., and Ng, N. L.: Chemical characterization of water soluble
1223 soluble organic aerosol in contrasting rural and urban environments in the
1224 Southeastern United States, *Environ. Sci. Technol.*, 51, 78-88, 2017.

1225 Zhang, Q., Alfara, M. R., Worsop, D. R., Allan, J. D., Coe, H., Canagaratna, M., and
1226 Jimenez, J. L.: Deconvolution and quantification of hydrocarbon-like and
1227 oxygenated organic aerosols based on aerosol mass spectrometry, *Environ. Sci.*
1228 *Technol.*, 39, 4938-4952, 2005.

1229 Zhang, Q. et al.: Ubiquity and dominance of oxygenated species in organic aerosols in
1230 anthropogenically-influenced Northern Hemisphere midlatitudes, *Geophys. Res.*
1231 *Let.*, 34, L13801, doi: 10.1029/2007gl029979, 2007.

1232

1233

1234

1235

1236

1237

1238

1239

1240

1241

1242

1243
1244
1245
1246
1247
1248
1249

1250
1251
1252
1253
1254
1255
1256
1257
1258
1259
1260
1261
1262
1263
1264
1265
1266
1267
1268
1269
1270
1271
1272
1273
1274
1275

Table 1. Average ambient concentration of each factor and total OA, and the corresponding fraction of the data above the threshold ($0.2 \mu\text{g m}^{-3}$).

Factor	Average Ambient Concentration ($\mu\text{g m}^{-3}$)	% of Measurements above the Threshold
MO-OOA	1.96	92
LO-OOA	1.66	96
Isoprene-OA	0.9	76
BBOA	0.5	42
Total OA	5.02	99

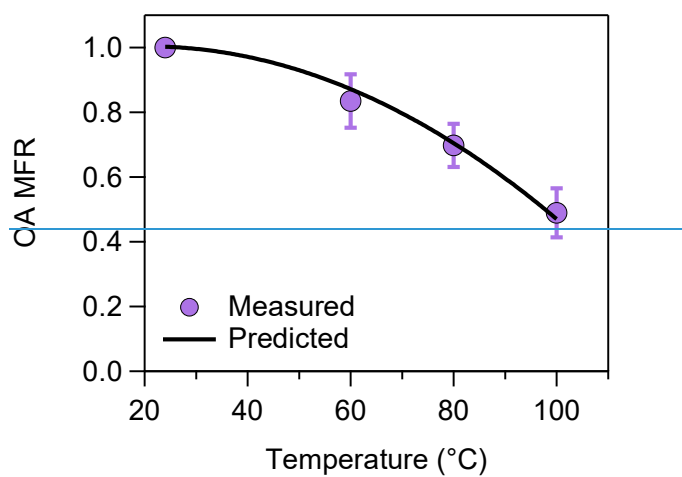
1276
1277
1278
1279
1280
1281
1282
1283
1284
1285
1286

Table 2. OA mass fractions of the ambient and ambient and +TD PMF factors.

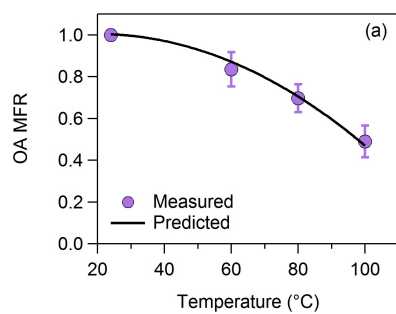
Data Used	MO-OOA	LO-OOA	Isoprene-OA	BBOA
	(%)	(%)	(%)	(%)
Ambient only	39	32	18	10
Ambient <u>and</u> +TD	43	29	19	9

1287
1288
1289
1290
1291
1292
1293
1294
1295
1296
1297
1298
1299
1300
1301
1302
1303
1304
1305
1306
1307
1308
1309
1310
1311
1312
1313
1314
1315
1316

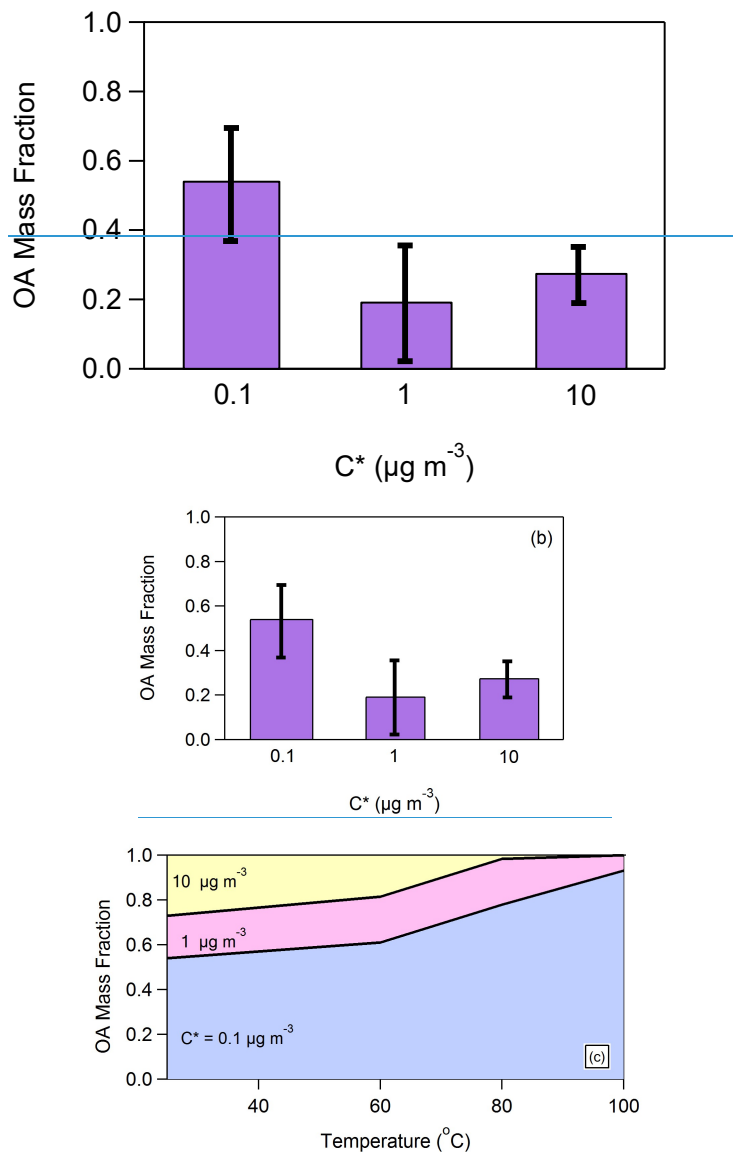
1317
1318
1319
1320
1321
1322
1323



1324



1325



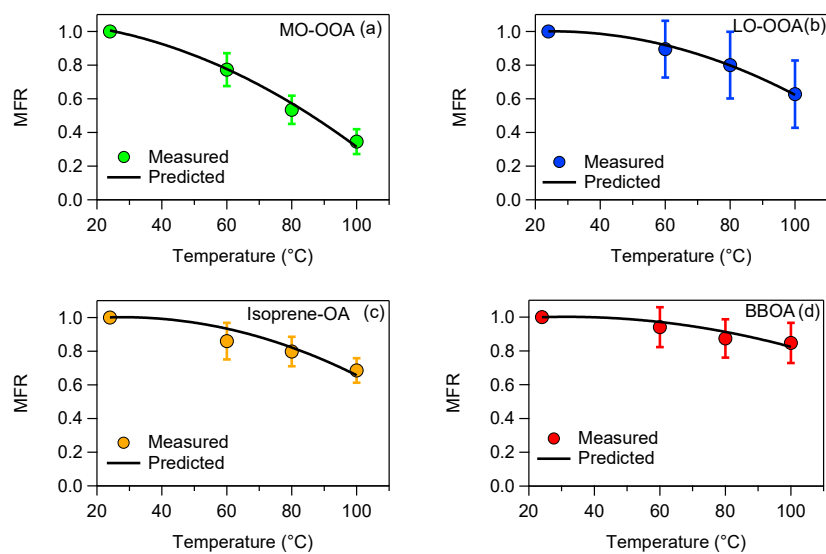
1326

1327

1328

1329 **Figure 1.** (a) Loss-corrected MFR of the total OA. The purple circles correspond to the
 1330 measurements and the uncertainties to one standard deviation of the mean. It is assumed
 1331 that MFR=1 at $T=24^{\circ}\text{C}$. The black line is the model fit estimated using the approach of

1332 Karnezi et al. (2014). (b) The total OA volatility distribution. The uncertainties have been
1333 estimated according to the algorithm of Karnezi et al. (2014). [\(c\) The predicted volatility](#)
1334 [distribution composition](#) after passing through the thermodenuder as a function of the
1335 [temperature](#).
1336



1337

1338

1339

1340 **Figure 2.** MFRs of the loss-corrected PMF OA factors. The circles represent the
1341 measurements with the one standard deviation of the mean. The black line corresponds to
1342 the best predicted MFR using the algorithm of Karnezi et al. (2014).

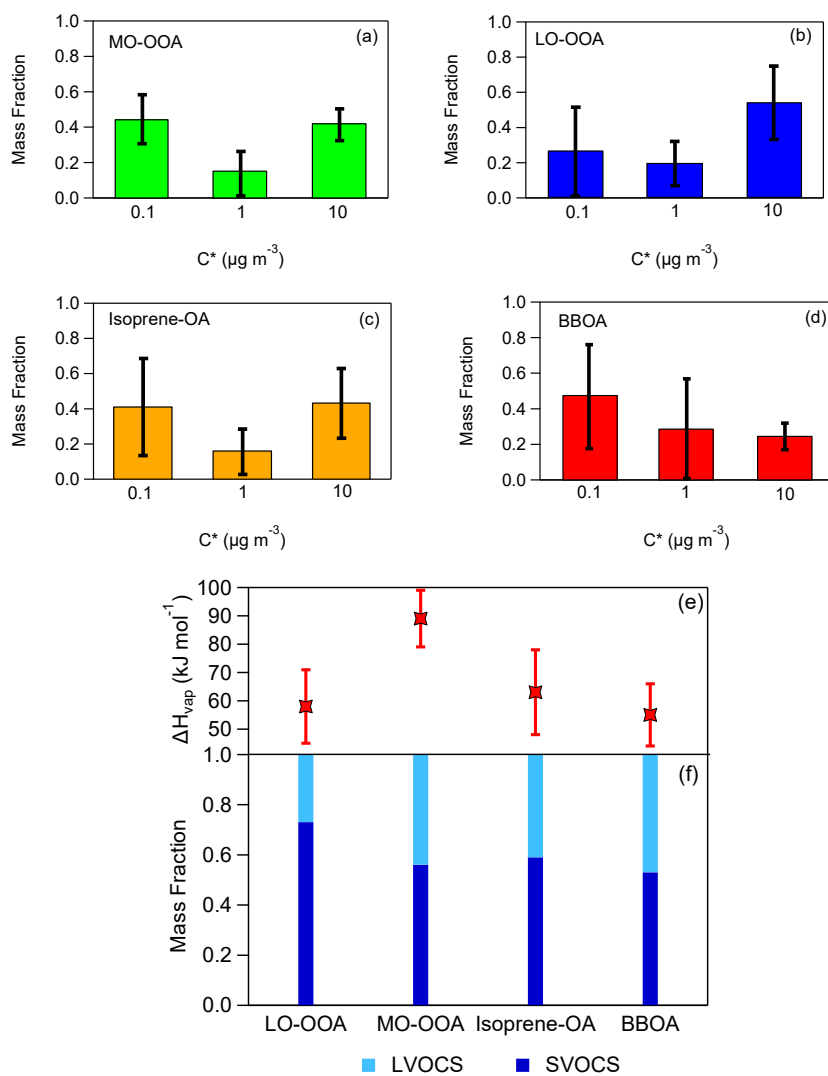
1343

1344

1345

1346

1347



1348

1349

1350

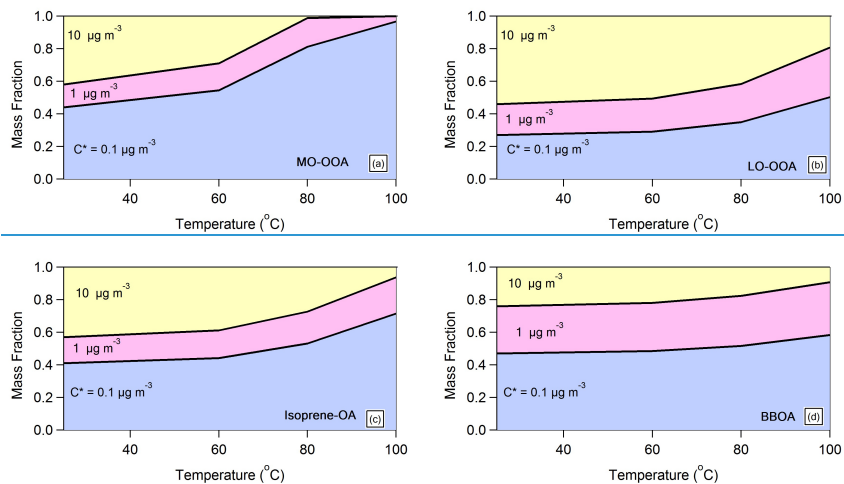
1351

1352 **Figure 3.** (a)-(d) Predicted volatility distributions of the OA PMF factors. The error bars

1353 correspond to the uncertainties derived using the approach of Karnezi et al. (2014), (e)

1354 vaporization enthalpies comparison between the four OA factors and (f) volatility

1355 compositions comparison between the four OA factors.



1356

1357

1358

1359

1360

1361

1362

1363

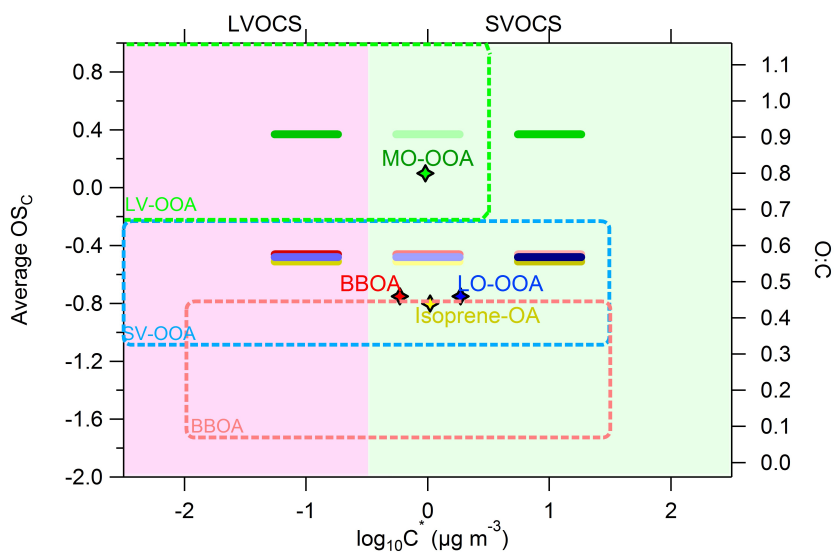
1364

1365

1366

1367

Figure 4. The predicted composition of the volatility distribution in terms of C^* of each factor after passing through the thermodenuder as a function of the temperature. The model predicts, as expected, that the less volatile material with $C^*=0.1 \mu\text{g m}^{-3}$ dominates the composition of the remaining aerosol after the TD as the temperature increases for all factors. However, there are significant differences in the evolution of the composition of the various factors.



1368

1369

1370

1371

1372

1373

1374

1375

1376

1377

1378

1379

1380

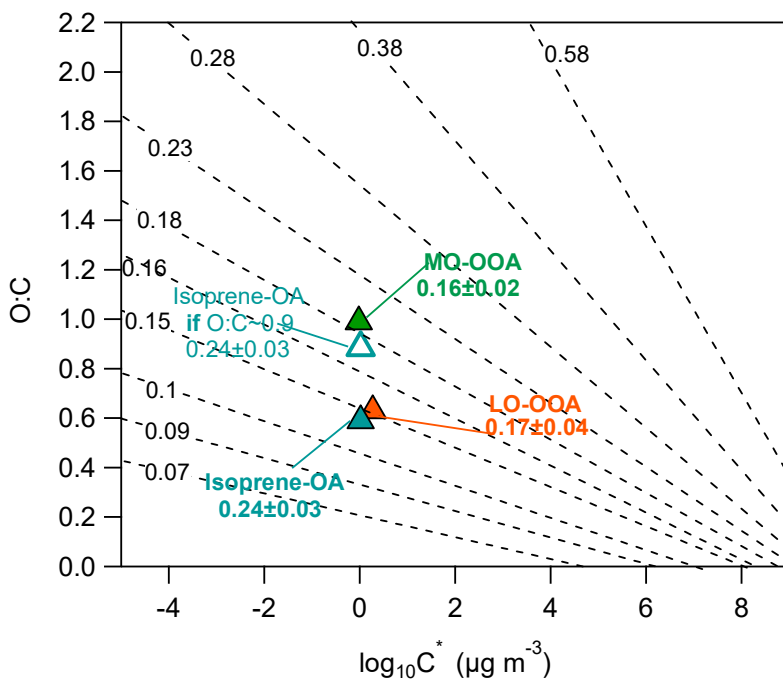
1381

1382

1383

1384

Figure 54. Average carbon oxidation state OS_C (left y axis) and O:C ratio (right axis) versus the saturation concentration in terms of $\log_{10}C^*$. The horizontal bars are the volatility distributions of the SOAS PMF factors: MO-OOA (green), LO-OOA (blue), Isoprene-OA (yellow) and BBOA (red). The darker the color of the horizontal bars the higher the mass fractional contribution for the corresponding C^* bin. The diamonds represent the average $\log_{10}C^*$ value for a given PMF factor. The green, light blue and pink dashed areas are the locations of the LV-OOA, SV-OOA and BBOA PMF factors as proposed by Donahue et al. (2012).

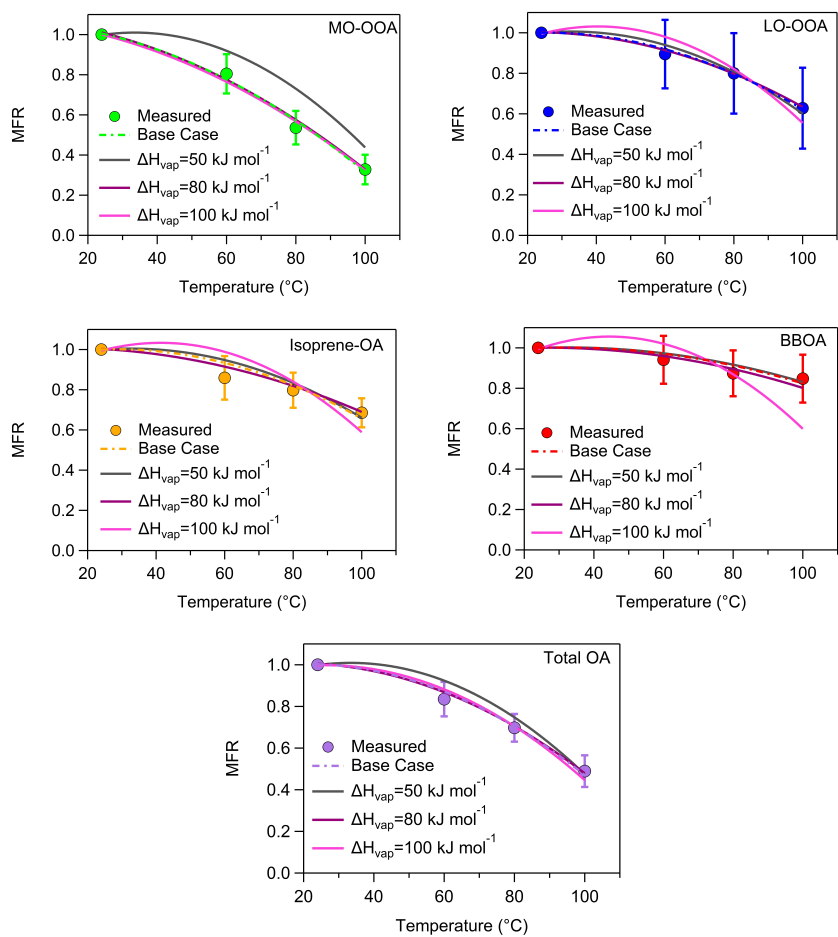


1385
 1386
 1387
 1388
 1389
 1390
 1391
 1392

Figure 65. O:C ratios versus the average volatility as $\log_{10}C^*$. The black isolines correspond to the theoretically intrinsic κ suggested by Nakao et al. (2017). The triangles denote the SOAS PMF factors. The hygroscopicity of the SOAS PMF factors has been transformed into the intrinsic κ , using the water solubility results of Xu et al. (2017). The open cyan triangle corresponds to the Isoprene-OA with a hypothetical O:C=0.9.

1393

1394 **Appendix**



1395

1396

1397

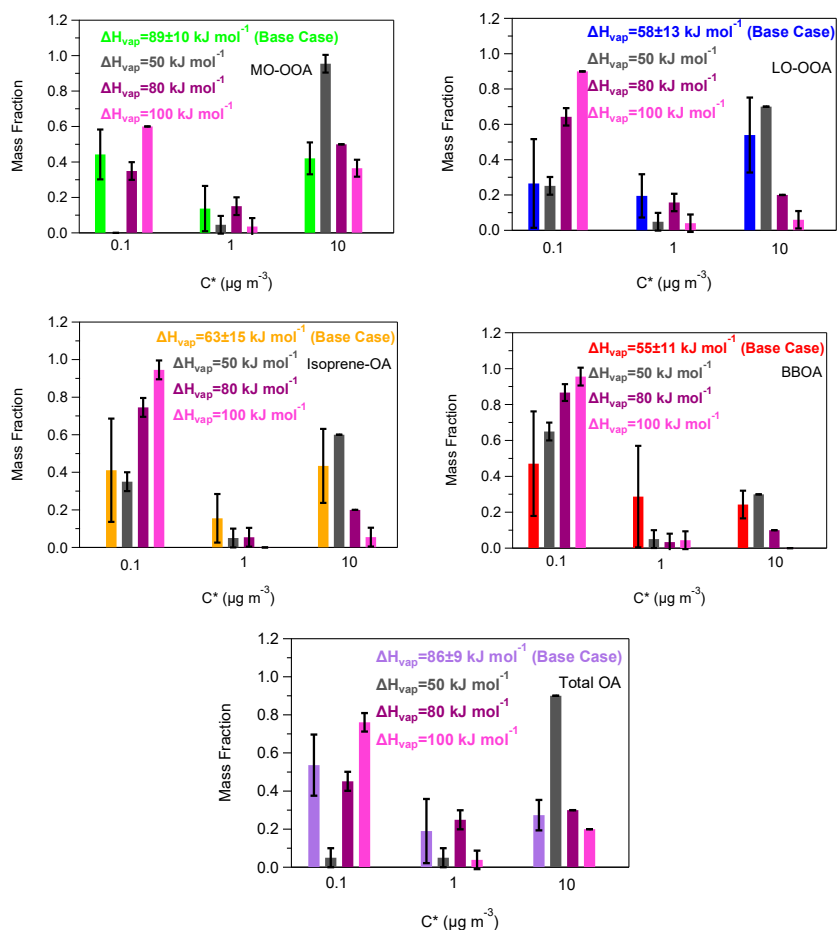
1398 **Figure A1.** MFRs of the loss-corrected PMF OA factors and total OA for fixed values of
1399 the vaporization enthalpy. The circles denote the measurements with the one standard
1400 deviation of the mean, the dash lines correspond to the base case, the grey lines represent
1401 the case of a constant ΔH_{vap} of 50 kJ mol^{-1} , the magenta lines stand for the case of a
1402 constant ΔH_{vap} of 80 kJ mol^{-1} and the pink lines correspond to the case of a constant
1403 ΔH_{vap} of 100 kJ mol^{-1} .

1404

Formatted: Font: Italic

Formatted: Font: Italic

Formatted: Font: Italic



1405

1406

1407

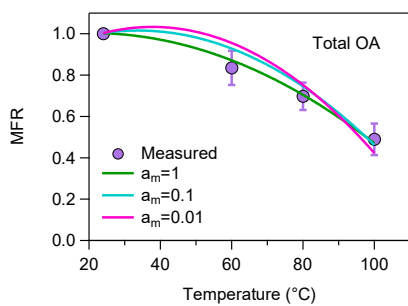
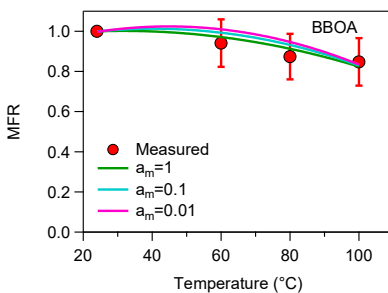
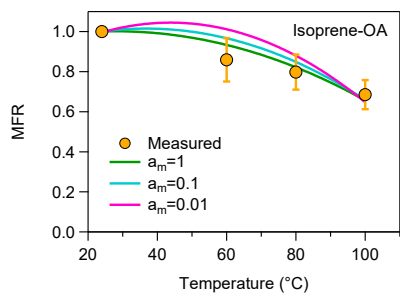
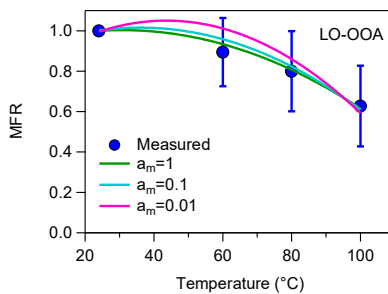
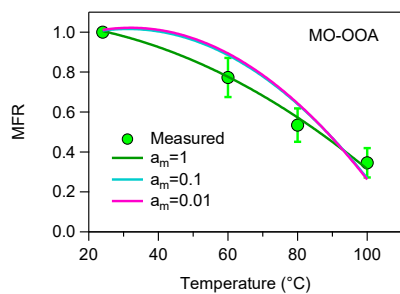
1408 **Figure A2.** Predicted volatility distributions of the OA PMF factors and total OA for
 1409 fixed vaporization enthalpy. The error bars are estimated using the approach of Karnezi et
 1410 al. (2014). The grey bars represent the results of a constant ΔH_{vap} of 50 kJ mol^{-1} , the
 1411 magenta bars correspond to the solution of a constant ΔH_{vap} of 80 kJ mol^{-1} , while and the
 1412 pink bars are the results for the case of a constant ΔH_{vap} of 100 kJ mol^{-1} . The green, blue,
 1413 orange, red and purple bars stand for the base case solutions of MO-OOA, LO-OOA,
 1414 Isoprene-OA, BBOA and total OA.

1415

Formatted: Font: Italic

Formatted: Font: Italic

Formatted: Font: Italic



1416

1417

1418

1419

1420

1421

1422

1423

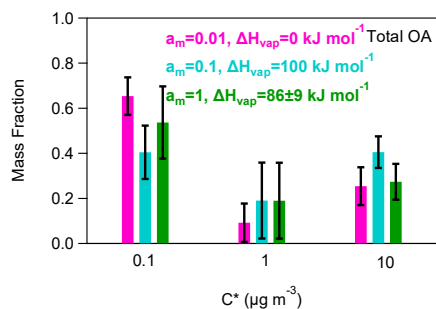
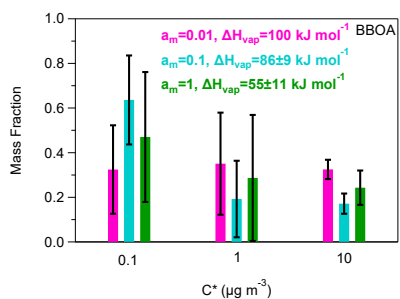
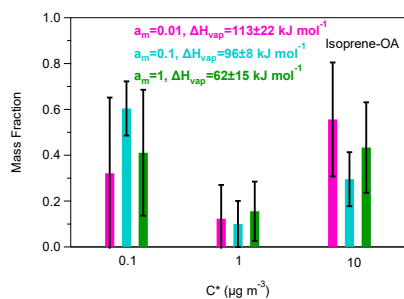
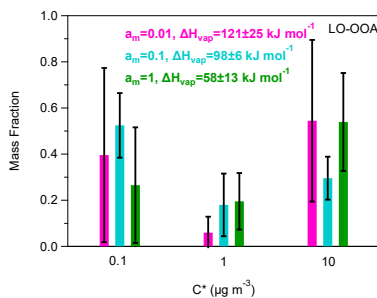
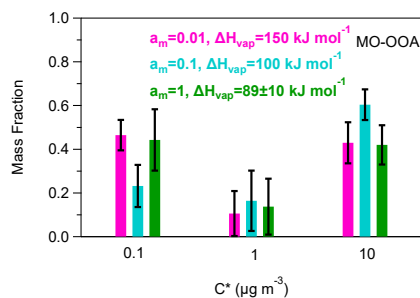
1424

Figure A3. MFRs of the loss-corrected PMF OA factors and total OA. The circles denote the measurements with the one standard deviation of the mean, the green lines represent the best predicted MFR for $a_m=1$ (base case), the cyan lines correspond to the best predicted MFR for $a_m=0.1$, while the pink lines stand for the predicted MFR for $a_m=0.01$.

Formatted: Font: Italic

Formatted: Font: Italic

Formatted: Font: Italic



1425

1426

1427

1428 **Figure A4.** Predicted volatility distributions of the OA PMF factors and total OA. The
 1429 error bars are estimated using the approach of Karnezi et al. (2014). The green bars
 1430 represent the results for $a_m=1$ (base case), the cyan bars correspond to the solution for
 1431 $a_m=0.1$, while and the pink bars are the results for $a_m=0.01$.

1432

Formatted: Font: Italic

Formatted: Font: Italic

Formatted: Font: Italic